AGU100 ADVANCING EARTH AND SPACE SCIENCE

Tectonics

RESEARCH ARTICLE
10.1029/2017TC004837

Key Points:
- Geochemical data reveal that both clinopyroxene- and amphibole-rich metagabbros are alkaline in composition
- There is no evidence in the gabbros of a high-pressure metamorphic event as previously suggested
- They were emplaced into crustal rocks during Early Triassic rifting of the northern margin of Gondwana

Supporting Information:
- Supporting Information S1
- Data Set S1

Correspondence to:
Y. Eyuboglu,
yenereyuboglu@gmail.com;
eyuboglu@ktu.edu.tr

Citation:
Eyuboglu, Y., Dudas, F. O., Chatterjee, N., Santosh, M., Billor, M. Z., & Yuva, S. (2018). Petrology, geochronology and tectonic setting of Early Triassic alkaline metagabbros from the Eastern Pontide Orogenic Belt (NE Turkey): Implications for the geodynamic evolution of Gondwana's Early Mesozoic northern margin. *Tectonics*, *37*, 3174–3206. https://doi.org/10.1029/2017TC004837

Received 5 OCT 2017
Accepted 10 AUG 2018
Accepted article online 27 AUG 2018
Published online 22 SEP 2018

Petrology, Geochronology and Tectonic Setting of Early Triassic Alkaline Metagabbros From the Eastern Pontide Orogenic Belt (NE Turkey): Implications for the Geodynamic Evolution of Gondwana's Early Mesozoic Northern Margin

Yener Eyuboglu[1], Francis O. Dudas[2], Nilanjan Chatterjee[2], M. Santosh[3,4], Mehmet Z. Billor[5], and Sabire Yuva[1]

[1]Department of Geological Engineering, Karadeniz Technical University, Trabzon, Turkey, [2]Department of Earth, Atmospheric and Planetary Sciences, Massachusetts Institute of Technology, Cambridge, MA, USA, [3]School of Earth Science and Mineral Resources, China University of Geosciences, Beijing, China, [4]Department of Geosciences, University of Adelaide, Adelaide, South Australia, Australia, [5]College of Sciences and Mathematics, Department of Geology, Auburn University, Auburn, AL, USA

Abstract The Triassic geodynamic evolution of the Pontides Belt, which geographically corresponds to northern Anatolia, is still a matter of debate. We present and interpret geological, petrographical, geochemical, and geochronological data from small, discordant, metagabbroic rocks exposed in the Tokat Massif. Field and petrographic characteristics distinguish four subgroups: (i) medium-grained, slightly lineated, clinopyroxene-rich metagabbros; (ii) fine-grained, nonlineated, clinopyroxene-rich metagabbros; (iii) medium-grained, nonlineated, brown amphibole-rich metagabbros; and (iv) medium-grained, slightly lineated, brown and blue amphibole-rich metagabbros. Magmatic kaersutites give $^{39}Ar/^{40}Ar$ plateau ages of 244.6 ± 0.5 and 243.16 ± 0.92 Ma and overlap the U-Pb age of titanite from a clinopyroxene-rich sample. Inherited zircons (~460, ~880, and ~2600 Ma) in fine-grained clinopyroxene-rich metagabbros indicate interaction with a range of crustal rocks during the intrusion. The blue amphiboles are magnesioriebeckites that formed during metamorphism or late-stage crystallization. Geochemical data, including whole rock major and trace element concentrations, and Sr-Nd-Pb isotope compositions reveal that both clinopyroxene- and amphibole-rich metagabbros are alkaline in composition but derived from distinct mantle sources. They are compositionally distinct from mafic igneous rocks in the contemporaneous Permo-Triassic Karakaya Complex that is well exposed in the western part of the Pontides Belt. Considering all data, we suggest that the Pontides Belt was shaped above a south dipping subduction zone during Permo-Triassic and the alkaline gabbros that were emplaced into crustal rocks during Early Triassic back-arc rifting of the northern margin of Gondwana.

1. Introduction

During the Triassic, assembly of the last supercontinent, "Pangea," which started to form in the Cambrian, was completed, and its rifting into two separate landmasses, Laurasia to the north and Gondwana to the south, began. The Triassic geographic position of the Pontides Belt, which corresponds to the northern part of Turkey and is divided tectonically into three subbelts, the western, central, and eastern Pontides, is still controversial. The Pontides Belt most commonly is assigned to Laurasia and its Triassic geodynamic evolution is ascribed to northward subduction of oceanic lithosphere from the south of the belt (e.g., Adamia et al., 1977; Catlos et al., 2013; Dilek et al., 2010; Okay & Sahintürk, 1997; Rice et al., 2009). In contrast, some researchers emphasize that the Pontides Belt belonged to Gondwana and, beginning in the Triassic, was shaped by southward subduction of Paleo-Tethyan lithosphere from Paleozoic to Cenozoic (Bektaş et al., 1999; Dewey et al., 1973; Eyuboglu et al., 2007, 2010, 2014; Eyuboglu, Chung, et al., 2011; Eyuboglu, Dudas, Santosh, Xiao, et al., 2016; Eyuboglu, Santosh, Bektaş, & Chung, 2011; Eyuboglu, Santosh, Dudas, et al., 2011; Şengör & Yılmaz, 1981).

In the Western and Central Pontides, Triassic time is mainly represented by the Karakaya Complex that comprises partly metamorphosed clastic and volcanic units (e.g., Genç, 2004; Okay, 2000; Okay et al., 1991; Okay &

Göncüoğlu, 2004; Pickett & Robertson, 1996; Sayit et al., 2010; Sayit & Göncüoğlu, 2009; Şengör & Yılmaz, 1981; Tekeli, 1981; Yılmaz et al., 1997). According to Yılmaz and Şengör (1981), Karakaya units were formed in a back-arc marginal basin that opened behind Pontides Belt during the southward subduction of Paleo-Tethyan lithosphere and closed by Late Triassic time during the Cimmerian orogeny. However, the most common interpretation is that Karakaya Complex represents a subduction/accretion prism that was accreted to the southern margin of Eurasia during the northward subduction of Paleo-Tethyan lithosphere (e.g., Okay, 2000; Okay et al., 2002; Pickett & Robertson, 1996; Sayit et al., 2010).

Although Triassic units are widespread in the western and central parts of the Pontides belt, the records of Triassic time in the Eastern Pontides Orogenic Belt are relatively limited. In the Amasya area situated in the southwestern corner of the Eastern Pontides Orogenic Belt, at the base of the nonmetamorphic Mesozoic sequence, there is a unit consisting mainly of weakly metamorphosed terrigenous sedimentary rocks of Triassic age (Alp's Karasenir Formation, 1972). Similarly, Ağar (1977) reported a unit including mainly terrigenous sedimentary rocks in the Pulur region (Karakaya Formation) and suggested that it is Triassic in age based on its stratigraphic relations. Eyuboglu, Santosh, Bektaş, and Chung (2011) indicated that mafic-ultramafic intrusions exposed in Aksalur village immediately southeast of Amasya city were emplaced into low-grade metamorphic lithologies of the Tokat Massif in Late Triassic time, based on field observations and zircon U-Pb age determinations. They also emphasized that these intrusions are petrographically and geochemically similar to Alaskan-type mafic-ultramafic intrusions, with an abundance of hydrous minerals (phlogopite and hornblende) and subduction-related geochemical signatures, suggesting the existence of a south dipping subduction zone below the Pontide Belt during the Late Triassic. Conversely, Catlos et al. (2013) reported ion microprobe zircon and baddeleyite ages from blue amphibole-bearing metagabbro bodies exposed in the Amasya region, suggesting igneous activity in the Late Permian/Early Triassic, followed by high-pressure/low-temperature metamorphism. They also suggested that metamorphism and deformation in the region are related to northward subduction and subsequent closure of the Paleotethyan ocean basin and accretion of the Karakaya units to the Laurasian continental margin. Other researchers have also emphasized that mafic igneous rocks exposed in the Amasya region have undergone blueschist metamorphism during the Triassic, based on the presence of blue amphiboles, but without mineral chemistry data (e.g., Rojay & Göncüoğlu, 1997; Tüysüz, 1996).

The Permo-Triassic forms a key time interval in the Tethyan evolution of the Eastern Pontides Orogenic Belt (NE Turkey) due to lack of systematic geological, geochemical, geochronological, and geophysical data from known exposures or several of Triassic rocks await for recognition. In this study, we provide an extensive data set to evaluate the origin, geodynamic setting, and metamorphic conditions of Early Triassic alkaline metagabbro bodies that occur as small intrusions within low-grade metamorphic lithologies of the Tokat Massif in the Eastern Pontides Orogenic Belt and are geochemically distinct from the other Karakaya rocks. We also discuss the Permo-Triassic geodynamic evolution of Northern Turkey in the light of new and old data.

2. Geological Background

Turkey is composed geologically of three main tectonic units including the Pontides Belt, the Anatolide-Tauride Block, and the Arabian Platform, from north to south (Figure 1). The Pontides Belt geographically corresponds to the northern part of Turkey and extends parallel to the southern coast of the Black Sea, between the Caucasus and the Carpathians (Figure 1). It is divided tectonically into three subbelts, the Western, Central, and Eastern Pontides. The Eastern Pontides Orogenic Belt, a mountain chain extending parallel to the southeastern coast of the Black Sea with a length of 550 km and a width of 200 km, is an essential part of the Alpine-Himalayan Belt (Figure 2). In the northern part of the belt, Late Mesozoic-Cenozoic volcanic and plutonic rocks are the dominant lithologies. Massive sulfide deposits (Eastern Black Sea-type Volcanogenic Massive Sulfide Deposits, Eyuboglu et al., 2014) associated with late Cretaceous tholeiitic to shoshonitic felsic volcanic rocks are the main economic occurrences in this area. The southern part is geologically interesting because of its numerous rock associations. Pre-Mesozoic metamorphic and granitic rocks are the Hercynian basement of the Eastern Pontides Orogenic Belt (including the Pulur, Ağvanis, and Tokat Massifs; the Kurtoğlu, Kopuzsuyu, Petekkaya, and Karadağ metamorphics; and the Köse and Gümüşhane granitoids). Alaskan-type mafic-ultramafic intrusions (Eyuboglu et al., 2010; Eyuboglu, Dudas, Santosh, Xiao, et al., 2016; Eyuboglu, Santosh, Bektaş, & Chung, 2011) span Carboniferous to Late Triassic time and were

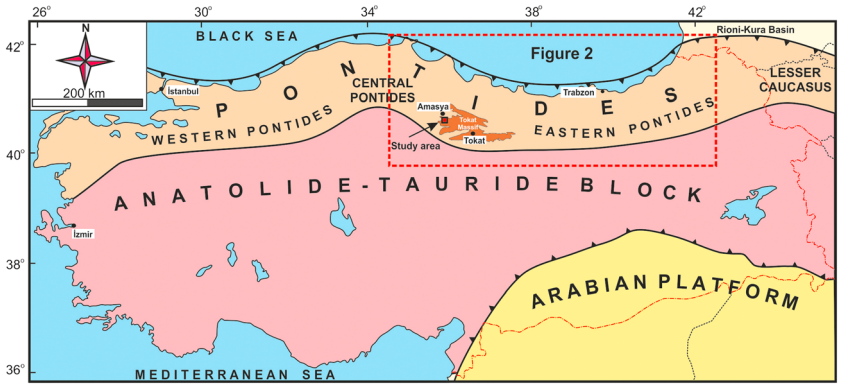

Figure 1. The main tectonic units of Turkey (modified from Ketin, 1966).

followed by numerous arc-related magmatic series: early to middle Jurassic tholeiitic to calc-alkaline felsic and mafic intrusions (Eyuboglu, Dudas, Santosh, Xiao, et al., 2016), late Cretaceous shoshonitic and ultrapotassic volcanic rocks (Eyuboglu, 2010; Eyuboglu, Chung, et al., 2011), late Paleocene-early Eocene

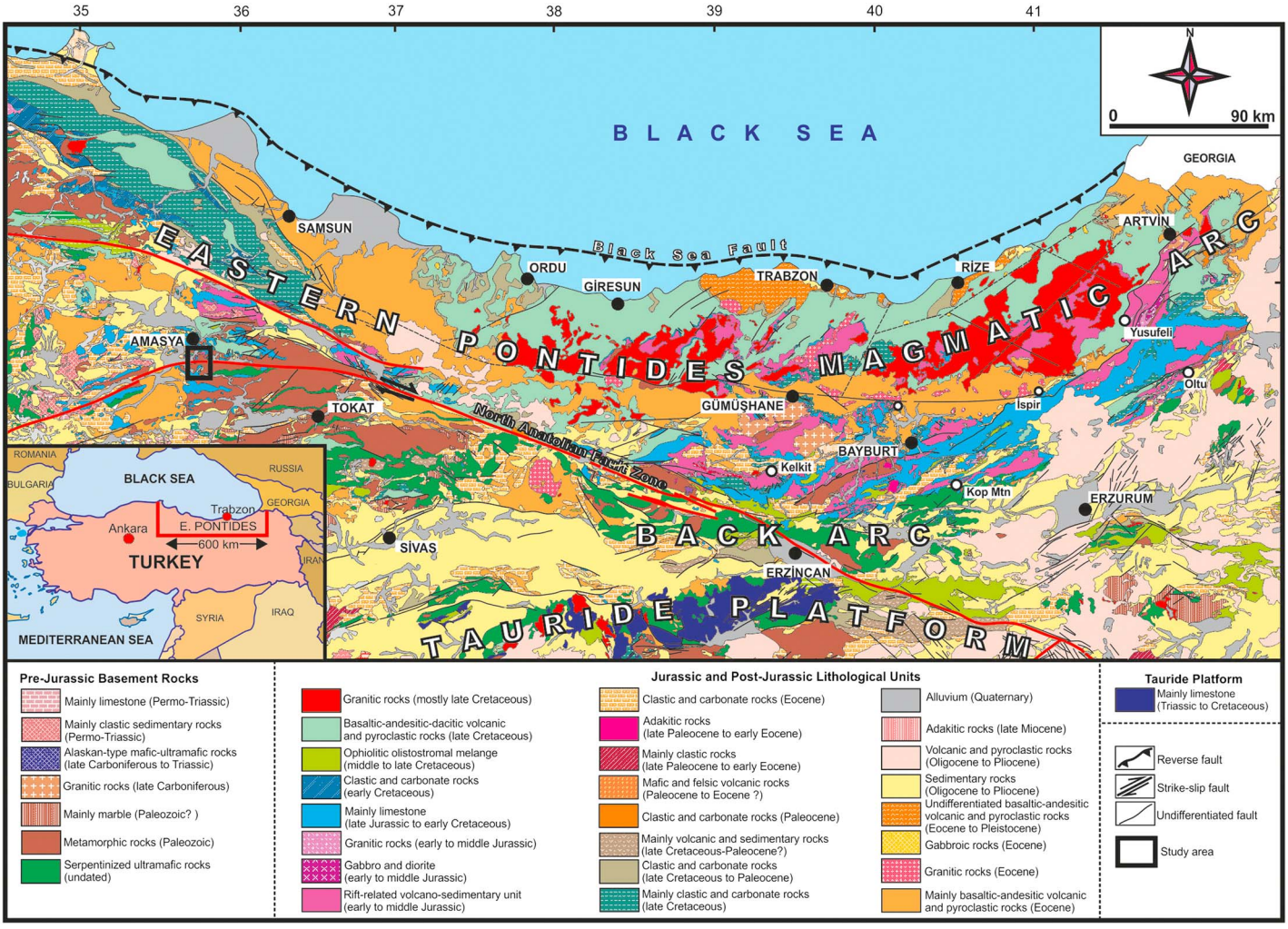

Figure 2. The main lithological units of the eastern Pontides Orogenic Belt (modified from 1/500.000 scale geological map of Turkey prepared by Mineral Research and Exploration Institute of Turkey; Eyuboglu, Dudas, Santosh, Zhu, et al., 2016).

adakitic intrusions (Eyuboglu, Chung, et al., 2011; Eyuboglu et al., 2018; Eyuboglu, Dudas, et al., 2013; Eyuboglu, Santosh, & Chung 2011; Eyuboglu, Santosh, Dudas, et al., 2011; Eyuboglu, Santosh, et al., 2013; Topuz et al., 2005), Lutetian nonadakitic granitic intrusions (Arslan & Aslan, 2006; Eyuboglu, Santosh, et al., 2013; Eyuboglu et al., 2017; Karslı et al., 2007; Kaygusuz & Öztürk, 2015), and late Miocene adakitic porphyries (Eyuboglu et al., 2012). Pre-Mesozoic ultramafic-mafic rocks (the Kop and Erzincan massifs), a Cretaceous ophiolitic olistostromal melange, and Miocene volcanic and pyroclastic rocks are widespread in the far southern part of the belt (Eyuboglu et al., 2007; Eyuboglu, Dudas, et al., 2013; Eyuboglu, Dudas, Santosh, Zhu, et al., 2016).

The study area is situated in the western extension of the Tokat Massif (Alp, 1972; Blumenthal, 1950; Eyuboglu, 2006; Eyuboglu, Santosh, Bektaş, & Chung, 2011; Özcan et al., 1980; Rojay, 1993; Tüysüz, 1996; Yuva, 2015). The most detailed mapping (1/25.000) and description of rock units were first completed by Alp (1972), who also interpreted the conditions of low-grade metamorphism for the Paleozoic rocks hosting the studied metagabbroic bodies. According to Alp (1972), the metamorphic rocks in the study area can be divided into a greenschist and a phyllite series. The phyllite series can be further subdivided into four units: ferruginous schists, quartz porphyries, basic metamagmatics, and a main phyllite series. These metamorphic lithologies are cut by Early Triassic mafic alkaline intrusions, which are the main subject of this study, and are unconformably covered by the Triassic Karasenir Formation, which consists mainly of slightly metamorphosed terrigenous sedimentary rocks and also includes lenticular limestone bodies that are fossiliferous and yield a Silurian age (Alp, 1972). Late Triassic time is represented by phlogopite or hornblende-bearing, Alaskan-type ultramafic-mafic intrusions that are well exposed in the southern part of the map area (Eyuboglu, Santosh, Bektaş, & Chung, 2011; Figure 3). The pre-Jurassic units are unconformably overlain by the basal conglomerate and terrigenous sedimentary rocks of the early to middle Jurassic Kayabaşı Formation in the northern part of the investigated area. The sequence grades upward into thin-medium bedded micritic limestones of the late Jurassic-early Cretaceous (Carcurum Formation). Early to middle Jurassic terrigenous sedimentary rocks are absent in the south of the studied area, where metamorphic rocks are directly covered by gray and beige colored, thick-bedded limestones of the late Jurassic-early Cretaceous Ferhatkaya Limestone (Eyuboglu, Santosh, Bektaş, & Chung, 2011). In the study area, the middle Cretaceous is represented by an olistostromal ophiolitic mélange. The basement rocks of the mélange comprise uplifted and eroded platform carbonate rocks of the late Jurassic-early Cretaceous (Eyuboglu et al., 2007). The contact between greenschist facies metamorphic rocks and the melange is tectonic in some areas (Eyuboglu, Santosh, Bektaş, & Chung, 2011). About 10 km north of the map area (Eyuboglu, 2010), the ophiolitic olistostromal mélange is covered by Campanian high-K volcanic and pyroclastic rocks. All of these units are unconformably covered by the Eocene Meşeliçiftlik Formation, consisting of andesitic pyroclastic rocks interbedded with clastic sedimentary rocks (Tüysüz, 1996).

3. Field Characteristics and Petrography

The studied metagabbroic bodies are well exposed around İlyasköy, approximately 13 km south of Amasya city center in the southwestern corner of the Eastern Pontides Orogeic Belt (Figures 2 and 3). Our detailed field and petrographic observations indicate that they can be classified into four subgroups: (i) medium-grained, slightly lineated, clinopyroxene-rich metagabbros; (ii) fine-grained, nonlineated, clinopyroxene-rich metagabbros; (iii) medium-grained, nonlineated, brown amphibole-rich metagabbros; and (iv) medium-grained, slightly lineated, brown and blue amphibole-rich metagabbros.

3.1. Medium-Grained, Slightly Lineated, Clinopyroxene-Rich Metagabbros

These metagabbroic rocks occur as small, oval, discordant intrusions within the metamorphic rocks and sometimes are stretched parallel to the dominant metamorphic foliation. They are generally massive and calcite-filled fractures are common. In hand specimen, the medium-grained rock is black due to its high clinopyroxene content (Figure 4), and slightly lineated due to a preferred orientation of slender clinopyoxene phenocrysts. In thin section, the rock consists predominantly of medium-grained (0.5–5 mm) clinopyroxene (about 70%), minor plagioclase, ilmenite and/or titanomagnetite, and interstitial sericite and chlorite (Figures 5 and 6). Slender phenocrysts of clinopyroxene have rounded terminations, and the grains are rimmed by chlorite. The mostly equigranular phenocrysts are slightly colored (tan), but nonpleochroic. Phenocrysts of mostly euhedral/subhedral zoned plagioclase are interstitial to the clinopyroxene

10.1029/2017TC004837

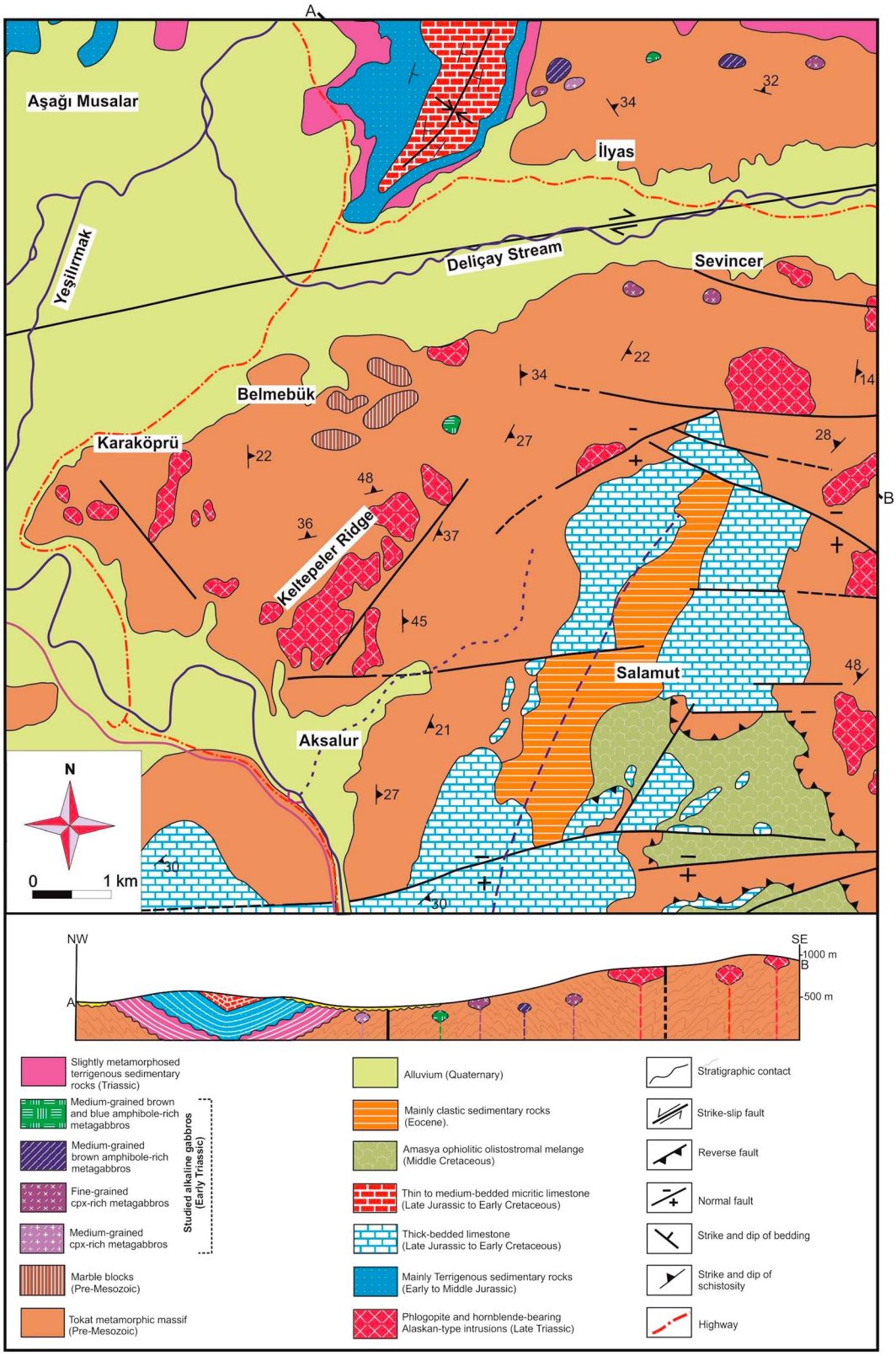

Figure 3. Geological map showing the distribution and crosscutting relationships of the metagabbroic intrusions in the study area (modified from Alp, 1972; Eyuboglu, Santosh, Bektaş, & Chung, 2011, and 1/100.000 scale geological map of Amasya prepared by Turkish Petroleum Company).

Figure 4. Representative field photos showing the contact relationships and field characteristics of metagabbros. (a) A sharp intrusive contact between fine-grained cpx-rich metagabbros and phyllites. (b) The medium-grained metagabbros are characterized by their well-developed fractures and blackish color due to high clinopyroene content. (c) Slender amphibole crystals in the medium-grained brown-amphibole-rich metagabbros.

phenocrysts, and some are partly or completely replaced by sericite and clinozoisite. Relatively coarse grained ilmenite or titanomagnetite is disseminated through the rock. Some grains are partly altered to leucoxene, and some of the coarse-grained aggregates are completely altered to titanite. Sericite is interstitial to the clinopyroxene phenocrysts, and evidently crystallized at the expense of interstitial plagioclase. Chlorite is interstitial to the clinopyroxene phenocrysts and also occurs as veins that fill some of the fractures in the grains. Much of the chlorite forms a narrow rim around the pyroxene. Fine-grained, granular epidote and clinozoisite are included in sericite-chlorite-rich domains. Titanite, pyrite, quartz, apatite, and zircon occur as accessory phases in the rock (Table 1).

3.2. Fine-Grained, Nonlineated, Clinopyroxene-Rich Metagabbros

These metagabbroic rocks occur as very small intrusive bodies (< 0.2 km^2) within the metamorphic lithologies of the Tokat Massif (Figure 3). Their contact with the host rocks is generally sharp (Figure 4). The rock is characteristically dark gray or greenish gray in hand specimen. Thin section studies of the rock reveal that it consists predominantly of clinopyroxene, amphibole, plagioclase, and titanomagnetite (Figures 5 and 6). Plagioclase occurs as lath-shaped phenocrysts with slightly subrounded terminations, as euhedral/subhedral, zoned phenocrysts and as anhedral grains interstitial to amphibole and pyroxene. Some is weakly sericitized. Slender, elongate clinopyroxene makes up a significant part of the rock (about 35%). As with plagioclase, most have subrounded terminations (Figure 5). They are generally nonpleochroic and are often twinned. Pleochroic brown amphibole phenocrysts occur in aggregates. Some grains are euhedral/subhedral, and pleochroism ranges between light tan to brown. Several brown amphiboles are rimmed and partly replaced by fine-grained blue/purple amphibole, or by chlorite. Anhedral grains of altered titanomagnetite are relatively abundant (about 6%) and they are generally interstitial to the silicates. Most are

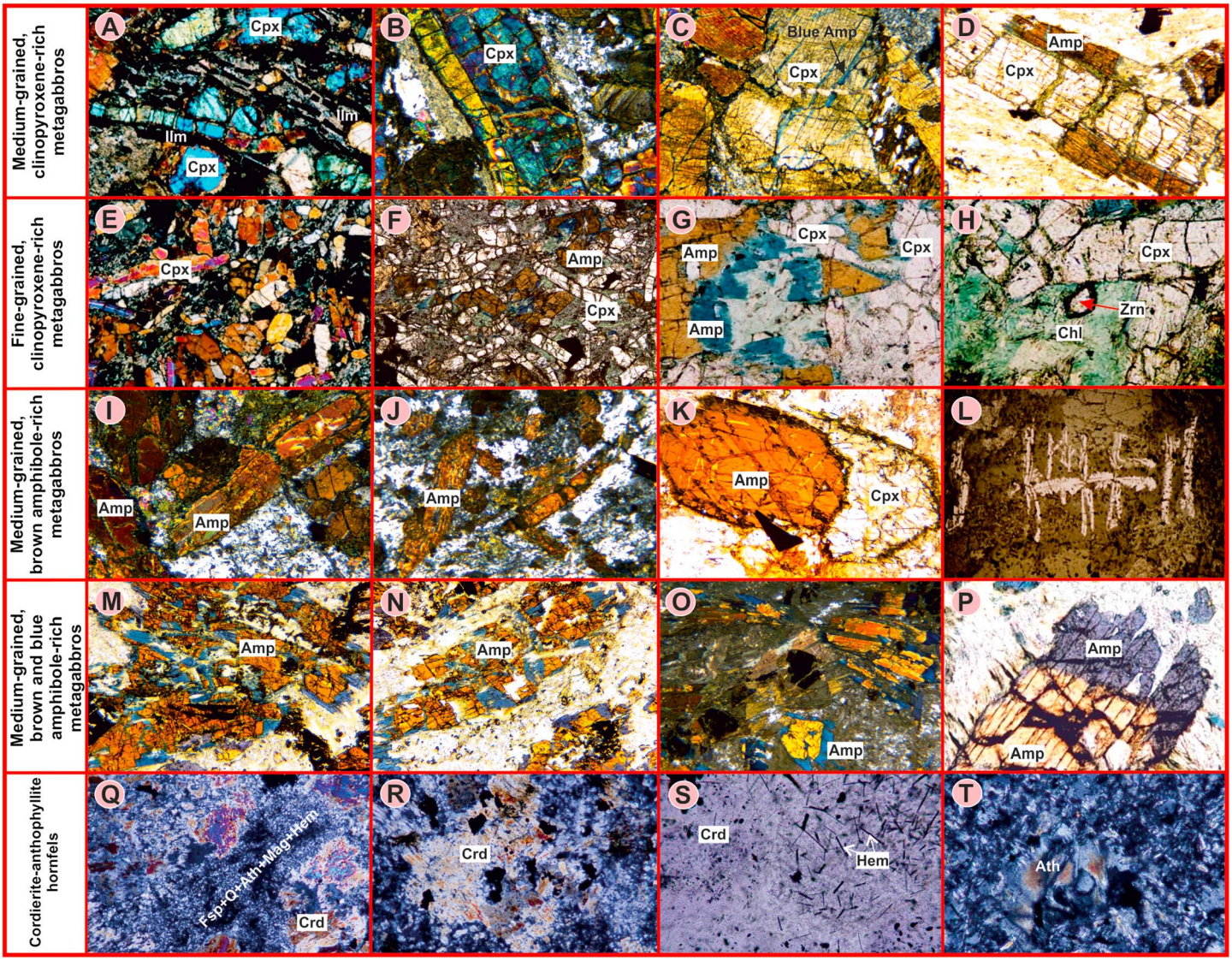

Figure 5. (a–d) From medium-grained, clinopyroxene-rich metagabbros; (e–h) from fine-grained, clinopyroxene-rich metagabbros; (i–l) from brown-amphibole-rich metagabbros; (m–p) from brown- and blue-amphibole-rich metagabbros; and (q–t) from cordierite-anthophyllite hornfels. (a) Long needles of ilmenite (black) are interstitial to clinopyroxene (*X* axis: 2.3 mm). (b) Fractures in a large clinopyroxene crystal (*X* axis: 1.6 mm). (c) Secondary blue amphibol fills fractures in clinopyroxene (*X* axis: 1.6 mm). (d) Pleochroic brown amphibole rims clinopyroxene (*X* axis: 1.6 mm). (e and f) Slender, elongate clinopyroxene crystals (*X* axis: 2.3 mm). (g) Brown amphibole is replaced by blue amphibole and chlorite (*X* axis: 2.3 mm). (h) Large zircon in chlorite (*X* axis: 0.45 mm). (i and j) Slender brown aphiboles (*X* axis: 1.6 mm). (k) Subrounded brown amphibole (*X* axis: 1.6 mm). (l) Typical ilmenite texture suggests rapid quenching (*X* axis: 2.3 mm). (m–o) Brown amphibole is partly replaced by blue amphibole in fractures (*X* axis: 1.6 mm). (p) Brown amphibole is rimmed by pleochroic purple amphibole. Pleochroism changes from purple to blue (*X* axis of photo: 0.45 mm). (q and r) Irregular porphyroblasts of cordierite in a matrix of finer-grained quartz, feldspar, anthophyllite, and opaque oxides (*X* axis: 2.8 mm). (s) Scattered hematite grains included in cordierite. (*X* axis: 0.7 mm). (t) Radiating aggregates of fibrous anthophyllite (*X* axis: 0.7 mm).

partly altered to leucoxene. Some contain inclusions of anhedral pyrite. Anhedral pyrite is fractured; some occur in aggregates and are generally associated with the partial replacement of amphibole by chlorite. Sericite is interstitial to the clinopyroxene and plagioclase phenocrysts, and probably crystallized from the breakdown of fine-grained, interstitial plagioclase. Chlorite forms a rim on some of the amphibole and is interstitial to the amphibole and pyroxene. Some are rimmed by and intercalated with blue amphibole. Clinozoisite, chalcopyrite, zircon, titanite, and apatite occur as accessory phases (Figure 5).

3.3. Medium-Grained, Nonlineated, Brown Amphibole-Rich Metagabbros

The body including this type of metagabbroic rocks is well exposed in upper elevations of Kavakağıl valley, about 1.5 km northwest of İlyasköy, and occupies an area of 0.3 km^2 (Figure 3). It has a sharp intrusive

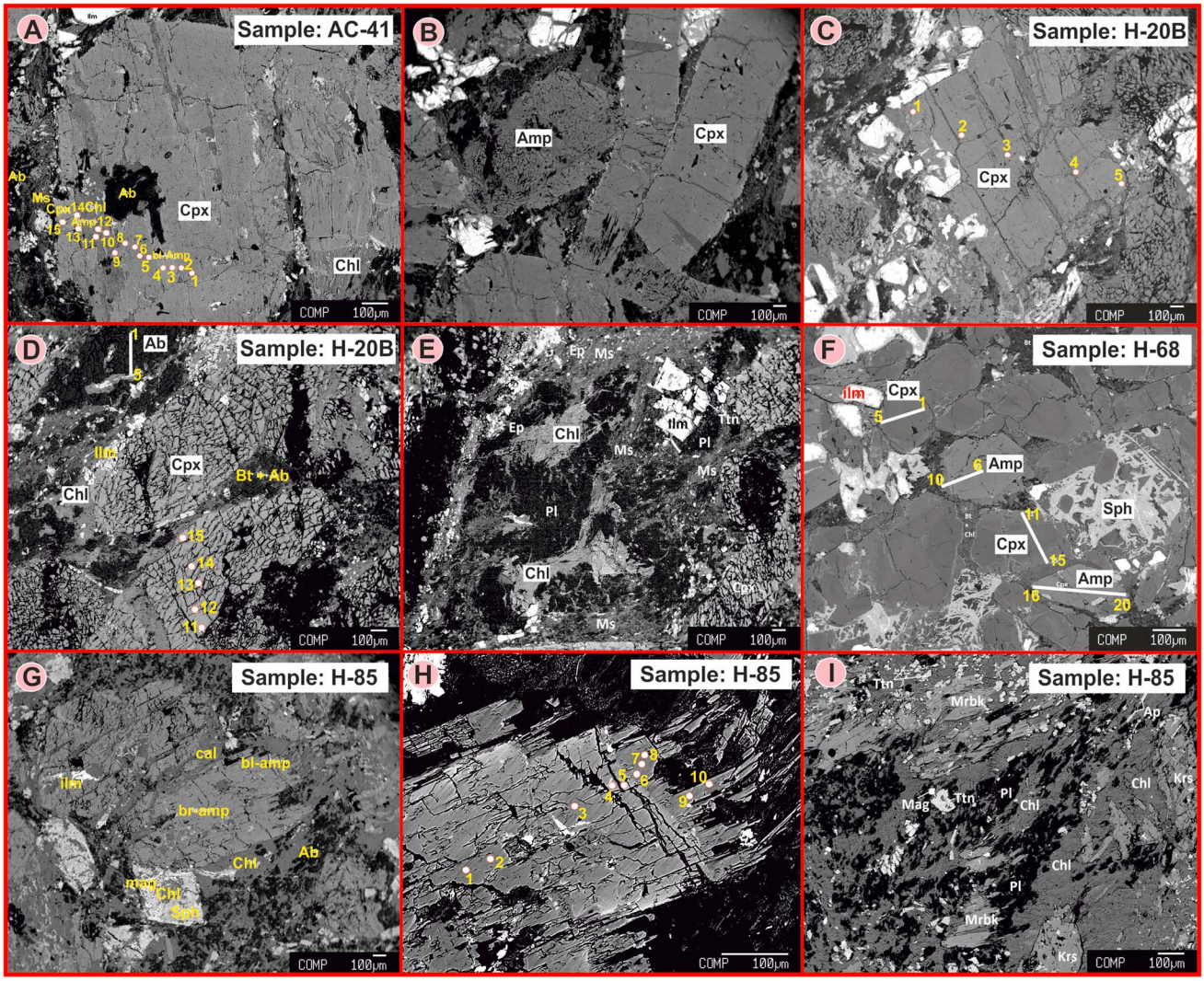

Figure 6. (a) A large clinopyroxene crystal with secondary magnesioriebeckite amphibole and chlorite veins and albite inclusion. Chlorite and albite also occur in the surrounding matrix. (b) Large clinopyroxene crystals and kaersutite amphibole. (c and d) Large clinopyroxene crystals surrounded by ilmenite grains, and a matrix composed of mica, chlorite, and albite. (e) Shape-preferred aggregates of chlorite and muscovite with granular epidote wrapping around large crystals of clinopyroxene, ilmenite, and albitic plagioclase. (f) Sample H-68 showing subhedral to euhedral grains of clinopyroxene and kaersutite amphibole with subordinate ilmenite and titanite (sphene). (g and h) Large tabular crystals of kaersutite amphibole with secondary calcite veins and rim overgrowths of magnesioriebeckite. Subordinate amounts of ilmenite and magnetite are intergrown with titanite (sphene), and the matrix contains chlorite and albite. (i) Parallel alignment of chlorite and magnesioriebeckite interspersed with fine-grained titanite and magnetite around albitic plagioclase relics and kaersutite.

contact with the phylites and calcschists of the Tokat Massif. In hand specimen, the medium-grained rock is characterized by an abundance of slender amphibole crystals (Figure 4). Thin section studies reveal that it consists predominantly of amphibole and plagioclase (Figures 5 and 6 and Table 1). The plagioclases are variably altered, and their twin lamellae destroyed. All of the large phenocrysts are partly replaced by clinozoisite and partly by fine-grained quartz. The altered plagioclase also contains long, needle-shaped apatite, some of which are overgrown by aggregates of fine-grained clinozoisite. Dark red, euhedral prismatic amphibole is strongly pleochroic, and some are partly replaced by chlorite and epidote. Some of the phenocrysts are completely altered to chlorite and epidote. Fine-grained, granular clinozoisite occurs as replacement after the plagioclase phenocrysts, and highly birefringent, fine- to medium-grained epidote aggregates appear to replace earlier mafic phenocrysts (amphibole or clinopyroxene). Chlorite aggregates form a rim on some of the amphibole phenocrysts. They are also intercalated with epidote and are interstitial to aggregates of epidote. Chlorite evidently represents partial replacement of mafic minerals. Skeletal ilmenite is disseminated through the rock. A few of the grains are partly altered to

Table 1
Visual Estimation of % Minerals in the Metagabbros

Rock type	Medium-grained, cpx-rich metagabbro	Fine-grained, cpx-rich metagabbro	Medium-grained, brown amphibole-rich metagabbro	Medium-grained, brown and blue amphibole-rich metagabbro
Plagioclase	5	25	28	
Quartz	x		3	3
Clinopyroxene	70	35		
Amphibole		20	40	55
Epidote[a]	2	x	7	5
Sericite	5	5		x
Chlorite	10	7	17	25
Carbonate				2
Apatite	x	x	x	x
Zircon	x	x	x	x
Titanite	x	x	x	2
Magnetite	4	6		8
Ilmenite	4		5	
Hematite				x
Pyrite	x	2		x
Chalcopyrite				x

Note. x: trace amount.
[a]Epidote or clinozoisite.

leucoxene—although most are unaltered. Fine-grained aggregates of anhedral quartz represent replacement after plagioclase phenocrysts. Apatite, zircon, and titanite occur as accessory phases in the rock (Table 1).

3.4. Medium-Grained, Slightly Lineated, Brown and Blue Amphibole-Rich Metagabbros

This type of metagabbroic rock occurs as bodies both discordant and concordant with the main foliation of the surrounding schists and phyllites. The discordant bodies are small (< 0.2 km^2) and circular. Crosscutting fractures are often filled with calcite and sometimes quartz. The concordant bodies occur as roughly laccolithic small intrusions (< 0.1 km^2). In hand specimen, the rock is characteristically blackish gray or dark green due to abundant amphibole phenocryts (about 55%). In thin section, the rock consists predominantly of amphibole (tan to reddish-brown pleochroism), blue-purple amphibole and a relative abundance of titanomagnetite (Figures 5 and 6). The replacement minerals include blue amphibole, clinozoisite, epidote, quartz, carbonate, chlorite, and titanite. Reddish-brown amphibole phenocrysts make up a significant part of the rock (about 45%). Most phenocrysts are fragmented and partly replaced by highly pleochroic blue/purple amphibole (riebeckite or glaucophane). The secondary amphibole forms a rim around the brown amphibole and develops along fractures. Fine-grained chlorite makes up a significant part of the rock (about 25%). It probably crystallized are the expense of the amphibole. Large domains of chlorite contain numerous inclusions of fine-grained clinozoisite, some carbonate, epidote, and minute titanite. Aggregates of fine-grained, granular clinozoisite probably crystallized at the expense of plagioclase phenocrysts. Fine-grained epidote is intercalated with clinozoisite and is also disseminated within chlorite-rich domains. Relatively coarse-grained (up to 0.6 mm) euhedral and subhedral titanomagnetite is rimmed by and partly replaced by fine-grained aggregates of titanite. Very fine grained, anhedral quartz is part of the replacement assemblage after the plagioclase phenocrysts. Aggregates of quartz are interstitial to the chlorite-rich domains. Fine-grained carbonate aggregates are part of the replacement assemblage after plagioclase. They occur within chlorite-rich domains and are intergrown with some of the epidote. Fine-grained titanite crystallized during the replacement of brown amphibole to blue amphibole. Zircon, sericite, pyrite, hematite, and apatite occur as accessory phases in the rock.

The contacts of the intrusions, where exposed, are sharp, but contact metamorphic zones around the intrusions are not distinct. This reflects, in part, the small size of the intrusions, and in part the unreactive nature of the host rocks. Cordierite-bearing hornfels has been recognized near contacts of two intrusions (Figure 5), and likely occurs in other locations as well.

4. Analytical Methods

The chemical compositions of minerals were measured on a JEOL JXA-8200 Superprobe electron probe microanalyzer at the Massachusetts Institute of Technology, Cambridge, United States, using an accelerating voltage of 15 kV, a beam current of 10 nA, and typical counting times of 20–40 s per element. A beam diameter of 1 μm was used for all minerals except plagioclase and amphibole, for which the beam diameter was 10 μm. A set of synthetic and natural mineral standards was used for calibration. The raw data were corrected for matrix effects using the CITZAF package (Armstrong, 1995). The standard deviations of the counts were $< 1\%$ for the major elements and ~1–5% for the minor elements, relative to the concentrations. Some additional analyses were carried out at the electron microprobe laboratories of the Geological Survey of Canada, where the instrument used was a Cameca SX-50 equipped with four spectrometers. The operating conditions were 20 kV, and 10 nA of probe current, with count times of 10 s on peak, and 5 s off-peak. Pyroxenes and oxides were acquired with a focused beam, and plagioclase and amphiboles were acquired with a larger, ~10- μm probe. The standards used were a mix of natural and synthetic metals and simple compounds.

Measurements of U, Th, and Pb of titanite grains extracted from a fine-grained clinopyroxene-rich metagabbro sample (SY-2) for U-Pb analysis were made using the Cameca IMS-1280 SIMS at the Institute of Geology and Geophysics, China Academy of Sciences (Beijing, China). Analytical details are described in Eyuboglu, Dudas, Santosh, Zhu, et al. (2016).

$^{40}Ar/^{39}Ar$ age determinations were carried out at the Auburn University Noble Isotope Mass Analysis Laboratory for samples H-84 and H-36 and at Géosciences Rennes (France) for sample AC-46. Analytical details are described in Özdamar (2016) and Ruffet et al. (1995), respectively.

Laser ablation inductively coupled plasma mass spectrometry (LA-ICP-MS) analysis for zircons from sample HS-2 was carried out at the *Key Laboratory of Crust-Mantle Materials and Environments, University of Science and Technology of China, Chinese Academy of Sciences*. Laser ablation was performed using an ArF excimer laser ablation system (193-nm wavelength), which was connected to an Agilent 7700E ICP-MS instrument. Helium was used as carrier gas in GeoLas system. The laser-generated aerosol was transported from the ablation cell to the ICP-MS instrument using a 1-m transfer tube with an internal diameter of 3 mm. Each analysis incorporates an approximately 24-s background acquisition (gas blank) followed by 40-s data acquisition from the sample. Every five sample analyses were followed by one analysis of NIST SRM 610 in order to correct the time-dependent drift of sensitivity and mass discrimination. Calibration was performed using NIST SRM 610 as external calibrant in conjunction with internal standardization using ^{29}Si. Internal standardization was used to correct for differences in the ablation rates between sample and reference material. Additionally, it also partially corrected for matrix effects and signal drift in the ICP-MS.

U-Pb isotopic analyses of four zircon grains extracted from sample HS-7 were also performed by LA-ICP-MS at the Department of Geosciences, National Taiwan University. Analytical details are described in Eyuboglu, Santosh, & Chung (2011).

Whole rock major and trace element analyses were performed on 35 samples at ACME Analytical Laboratories, Vancouver, Canada. The major oxides and Sc were determined using ICP-emission spectrometer (ES), and trace and rare earth elements were analyzed by ICP-MS. The sample digestion procedures are similar for both ICP-MS and ICP-ES; 0.2 gm of pulverized sample is weighed into a graphite crucible and mixed with 1.5 gm of $LiBO_2$ flux. The mixture is heated in a muffle furnace for 15 min at 1050 °C. The molten mixture is removed and quickly poured into 100 ml of 5% HNO_3. This solution is shaken for 2 hr, and the aliquot is transferred into a polypropylene test tube. Standards and reagent blanks are added to the sample sequence. At the second stage (sample analysis), sample solutions are aspirated into an ICP-MS (Perkin-Elmer Elan 6000) or an ICP-ES (Jarrel Ash Atomcomp Model 975) for determination of element content.

The Rb-Sr, Sm-Nd, and Pb isotopic ratios of five samples (SY-2, SY-3, SY-4, SY-5, and SY-6) were measured on a thermal ionization mass spectrometer (isoprobe-T) at the Korea Basic Science Institute (South Korea). Similarly, Rb-Sr, Sm-Nd, and Pb isotopic ratios of samples H-63, H-65, and H-85 were measured on a thermal ionization mass spectrometer (Finnigan MAT-262) at the Institute of Geology and Geophysics, China Academy of Sciences, Beijing, China. In addition, Rb-Sr, Sm-Nd, and Pb isotopic ratios of some samples (H-2, H-58, H-66, H-68, H-83, H-91, and H-92) were measured using the VG AXIOM MC-ICP-MS at School of

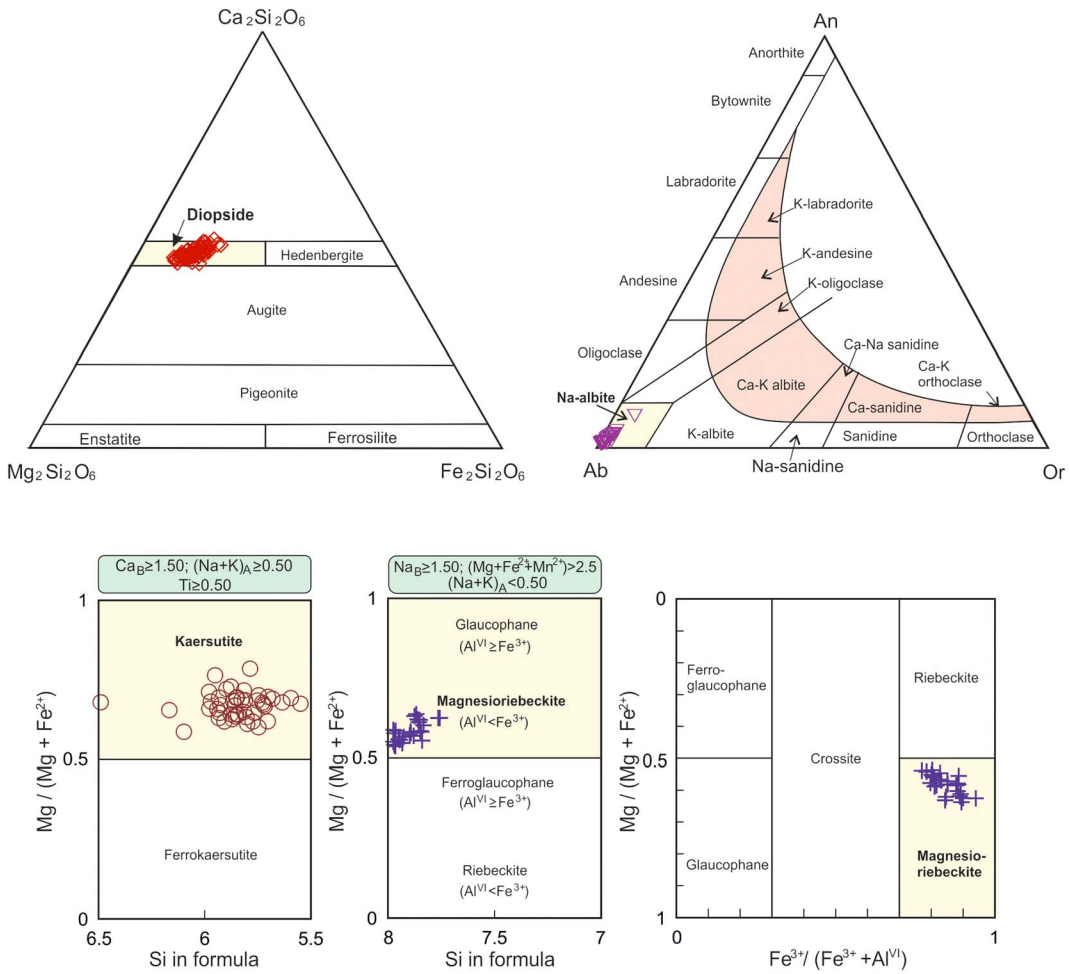

Figure 7. Chemical classification diagrams for pyroxenes (after Morimoto et al., 1988), plagioclases (after Smith & Brown, 1988), and amphiboles (after Leake et al., 1997).

Earth and Space Sciences, Peking University, Beijing, China. Analytical details are described in Eyuboglu, Dudas, Santosh, Xiao, et al. (2016), Eyuboglu (2010), and Eyuboglu (2015), respectively.

5. Results

5.1. Mineral Chemistry

5.1.1. Clinopyroxene

Representative clinopyroxene compositions are given in Table S1 in the supporting information and shown in Figure 7. Clinopyroxenes from both medium-grained and fine-grained clinopyroxene-rich metagabbros have similar major element concentrations and all plot in the diopsite field of the Wo-En-Fs ternary. They contain 44.52–51.03 wt.% SiO_2, 1.25–3.57 wt.% TiO_2, 2.48–8.19 wt.% Al_2O_3, 5.42–9.07 wt.% FeO_T, 10.83–15.14 wt.% MgO, and 20.82–23.83 wt.% CaO (Table S1). Concentrations of Cr_2O_3 (≤0.26 wt.%), MnO (≤0.24 wt.%), Na_2O (≤1.03 wt.%), and K_2O (≤0.03 wt.%) are low. Some clinopyroxenes display compositional zoning from TiO_2, Al_2O_3 and FeO-rich rims to TiO_2-, Al_2O_3-, and FeO-poor cores (Figure 7 and Table S1). The clinopyroxenes have high Mg numbers (100 × Mg/[Mg + Fe^{2+}]), varying between 76 and 98.

5.1.2. Amphibole

Representative amphibole compositions are presented in Table S2 and are shown in Figure 7. There are two main types of amphibole in the studied gabbroic rocks. Brown amphiboles have high concentrations of TiO_2 (4.01–7.20 wt.%). They also contain 36.74–44.81 wt.% SiO_2, 9.80–14.18 wt.% Al_2O_3, 10.11–14.75 wt.% FeO_T, 10.92–14.09 wt.% MgO, 8–65 wt.% 12.41 wt.% CaO, and 2.18–4.03 wt.% Na_2O and low concentrations of MnO (≤0.26 wt.%), Cr_2O_3 (≤0.09 wt.%), and K_2O (≤1.32 wt.%). On a diagram of Si versus Mg number

($100 \times Mg/[Mg + Fe^{2+}]$; Leake et al., 1997), brown amphiboles plot in the kaersutite field, with Si ranging from 5.70 to 6.49 and Mg numbers ranging from 59 to 77 (Figure 7). The blue amphiboles are sodic, with high Na_2O contents (4.42–8.09 wt.%; Table S2). Compared with the brown amphiboles, they have high concentrations of SiO_2 (53.12–56.04 wt.%) and FeO_T (21.67–24.77 wt.%), with low concentrations of TiO_2 (0.01–0.45 wt.%), Al_2O_3 (1.81–2.56 wt.%), MgO (7.86–10.25 wt.%), CaO (0.09–4.42 wt.%), MnO (≤0.17 wt.%), and K_2O (≤0.15 wt.%). Their Mg numbers range from 54 to 64 (Table S2). On the diagrams used for chemical classification of sodic amphiboles (Leake et al., 1997), the blue amphiboles are magnesioriebeckite (Figure 7): the high proportion of Fe^{3+} is diagnostic.

5.1.3. Plagioclase

Representative plagioclase compositions are presented in Table S3 and graphically shown in Figure 7. All plagioclases are albite, with high Na_2O (10.91–12.88 wt.%) and low CaO (≤0.41 wt.%) and K_2O (≤0.21 wt.%) contents. The SiO_2 and Al_2O_3 contents are 64.65–69.59 wt.% and 18.10–19.56 wt.%, respectively (Table S3).

5.1.4. Fe-Ti Oxides

Representative ilmenite and magnetite compositions are presented in Table S3. Ilmenites contain 43.04–48.99 wt.% TiO_2, 40.40–49.78 wt.% FeO_T, and 2.85–4.15 wt.% MnO and low concentrations of Al_2O_3 (≤0.91 wt.%). Magnetites are characterized by low concentrations of TiO_2 (0.44–1.68 wt.%), Al_2O_3 (0.19–0.32 wt.%), and MnO (0.02–0.07 wt.%) and high concentrations of FeO_T (88.14–91.27 wt.%).

5.1.5. Chlorite

Thin section studies revealed that chlorite makes up 10–25 vol. % of the studied rocks and evidently replaces amphibole and clinopyroxene. Representative chlorite compositions are presented in Table S3. Their SiO_2, Al_2O_3, FeO_T and MgO contents are 25.38–29.41, 15.82–18.82, 23.08–26.64, and 14.65–20.30 wt.%, respectively.

5.2. Geochronology

Analytical data for all geochronological analyses are included in Table S4. Titanite grains from SY-2, a fine-grained clinopyroxene gabbro, were analyzed for U and Pb isotopes. These analyses (Figure 8a) constrain the age of the gabbro to the Late Permian, at 256 ± 23 Ma (2 σ). The large uncertainty in part reflects the difficulty of making common Pb corrections to phases that incorporate Pb at the time of crystallization.

$^{39}Ar/^{40}Ar$ step-heating measurements on amphibole from AC 46 and H 84, samples of the brown amphibole-rich gabbros, yield Triassic plateau ages of 244.6 ± 0.5 Ma (2 σ; eight contiguous steps,> 75% of total Ar) and 243.16 ± 0.92 Ma (2 σ; 11 contiguous steps, 59% of total Ar), respectively (Figure 8b). These are the most precise age determinations we have of the metagabbros in this study. Step-heating $^{39}Ar/^{40}Ar$ measurement of amphibole from H 36, a sample containing both brown and blue amphibole, does not yield a plateau age (Figure 8b). The best estimate of its age is 238.1 ± 0.96 (2 σ) Ma, based on ~34% of the total Ar released in four contiguous, concordant steps in the analysis. The total gas age is 229.7 ± 13 Ma.

We attempted to date zircon from two samples of the fine-grained clinopyroxene gabbro (relevant data and figures are in Table S4 and Figure S1). The apparent ages were scattered, averaging near 880 Ma in H-2 ($n = 4$) and 460 Ma in H-7 ($n = 4$). Two analyses in H-2 yielded strongly discordant Archean ages ($^{207}Pb/^{206}Pb$ ages ~2600 Ma).

5.3. Whole Rock Geochemistry

5.3.1. Major Elements

We report data for 35 samples (Table S5; Table S6 includes normative compositions), with seven or more analyses from each of the four petrographically distinguished gabbro types. A major element classification diagram is shown in Figure 9a. The most striking features of the data are that the rocks are generally SiO_2 poor ($40.52 < SiO_2 < 46.01$ wt. %) and contain low Al_2O_3 (26 of 35 < 14 wt. %). The clinopyroxene-rich gabbros have the lowest SiO_2 and Al_2O_3 contents. Conversely, MgO, $Fe_2O_3(t)$ and CaO are high, ranging up to 13.2, 14.5, and 14.9 wt. %, respectively. Whole rock Mg numbers vary from 64 to 69 for the fine-grained pyroxene-rich gabbros, are between 57 and 63 for medium-grained pyroxene-rich and blue and brown amphibole-rich gabbros, and are between 46 and 51 for the brown amphibole-rich gabbros. Na_2O and K_2O are variable in comparison to the other major elements, with coefficients of variation>50%. Na_2O is particularly elevated (> 4.27 wt. %) in the brown amphibole-bearing gabbros, whereas the other three gabbro types have $Na_2O < 2.83$ wt. %. All gabbros contain $TiO_2 > 3.82$ wt. %, a remarkably high value for gabbroic

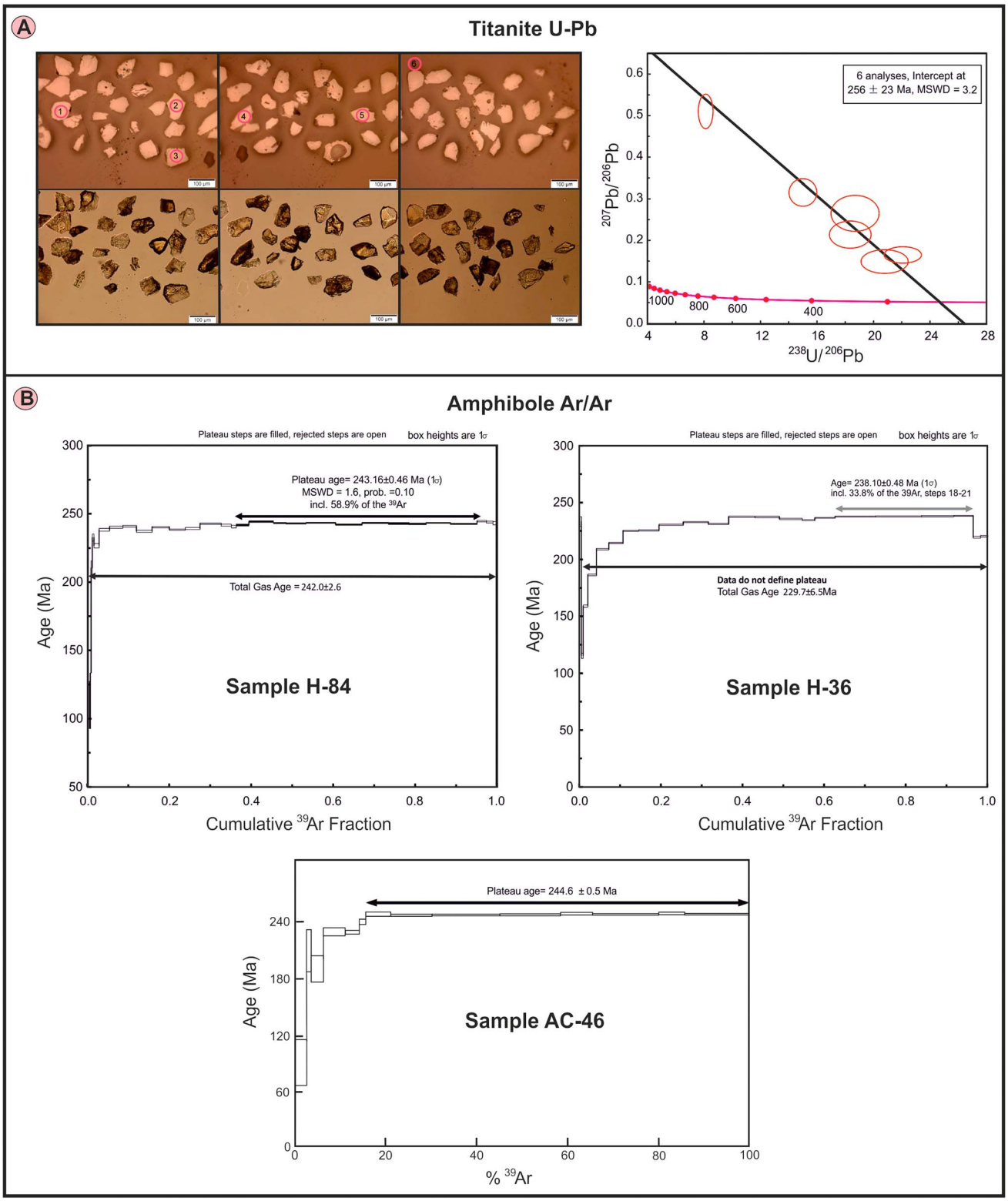

Figure 8. (a) Transmitted light photomicrographs and U-Pb Tera-Wasserburg plot of titanites separated from SY-2. (b) Diagrams for ^{40}Ar-^{39}Ar step-heating dating of magmatic amphiboles found in amphibole-rich metagabbros.

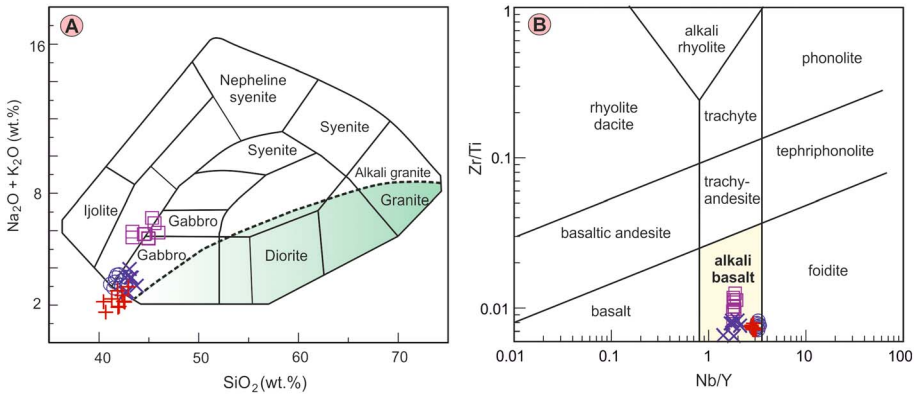

Figure 9. Chemical classification diagrams for Triassic metagabbros. (a) Total alkali versus SiO_2 (after Cox et al., 1979); (b) Zr/Ti versus Nb/Y (after Pearce, 1996).

rocks. Alteration of the gabbros, based on loss-on-ignition, is moderate (1.6–4.8 wt. %), with the highest values in the brown and blue amphibole-bearing gabbros.

5.3.2. Trace Elements

Trace element data for all samples are also shown in Table S5 and plotted in Figures 9b and 10. The large-ion-lithophile elements (LILE, including Ba, Cs, Pb, Rb, and Sr, in addition to K) generally have low but variable concentrations. The compatible 3-D transition metals that are commonly associated with MgO (Co $<$ 69, Cr $<$ 1,220, Ni $<$ 153 ppm) mostly have elevated concentrations, whereas those commonly associated with FeO (Mn and V) are not unusual ($<$ 0.20 wt.% MnO and $<$ 500 ppm V). The incompatible trace elements, including most of the high-field strength elements (HFSE; Hf, Nb, Ta, Ti, Y, and Zr) mostly have elevated concentrations. In multielement variation diagrams (Figures 10a and 10c), the abundances of most elements show a convex-upward pattern, with systematic depletions in most of the LILE. The scatter of LILE in the amphibole-bearing gabbros is greater than it is in the clinopyroxene gabbros.

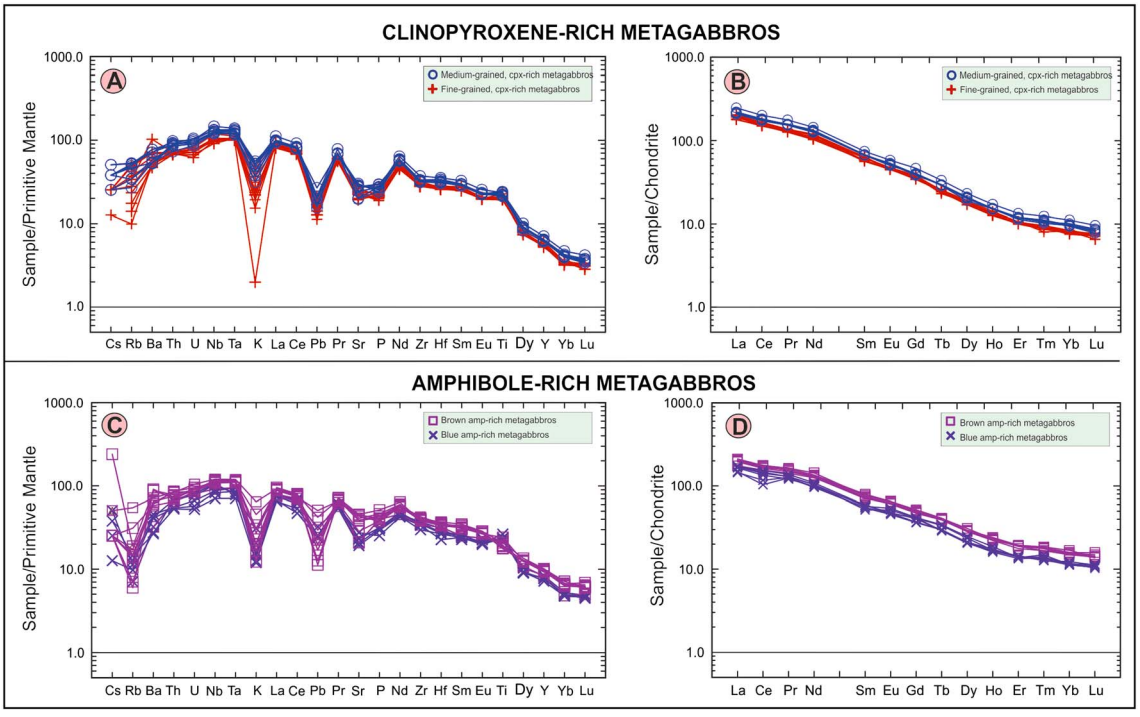

Figure 10. Primitive mantle-normalized trace (a, c) and chondrite-normalized rare earth element distribution patterns (b, d) for the metagabbros (primitive mantle values: Sun & McDonough, 1989; chondrite values: Boynton, 1984).

Table 2
Sr, Nd, and Pb Isotopic Compositions for the Studied Metagabbros

Sample	Rock type	Rb	Sr	$^{87}Rb/^{86}Sr$	$^{87}Sr/^{86}Sr$	$^{87}Sr/^{86}Sr$ (i)	Sm	Nd	$^{147}Sm/^{144}Nd$	$^{143}Nd/^{144}Nd$	$^{143}Nd/^{144}Nd$(i)
H-2	Fine-grained cpx-rich	6.3	512.5	0.036	0.703733	0.703612	12.1	65.4	0.1124	0.512629	0.512453
H-68	Fine-grained cpx-rich	21.5	479.5	0.130	0.704255	0.703813	11.28	69.3	0.0988	0.512650	0.512494
SY-2	Fine-grained cpx-rich	17.1	588.1	0.084	0.705183	0.704896	12.08	65.2	0.1125	0.512651	0.512474
SY-3	Fine-grained cpx-rich	25.4	461.7	0.159	0.704672	0.704129	10.95	59.1	0.1125	0.512651	0.512474
SY-4	Fine-grained cpx-rich	30.3	400	0.219	0.704848	0.704100	11.53	61.9	0.1131	0.512652	0.512474
SY-5	Fine-grained cpx-rich	24	470	0.148	0.704524	0.704020	11.3	61.5	0.1116	0.512657	0.512482
H-58	Medium-grained cpx-rich	36	633.8	0.164	0.704727	0.704166	13.23	77.5	0.1037	0.512652	0.512489
H-63	Medium-grained cpx-rich	33.7	414	0.235	0.704627	0.703823	13.22	78.8	0.1019	0.512654	0.512494
H-65	Medium-grained cpx-rich	31.1	597.3	0.151	0.704711	0.704197	13.05	78.0	0.1016	0.512661	0.51250 1
H-66	Medium-grained cpx-rich	21.6	608.3	0.103	0.704685	0.704334	13.03	76.4	0.1036	0.512645	0.512482
H-85	Blue and brown amp-rich	7.31	465.6	0.045	0.703279	0.703124	11.57	55.44	0.1267	0.512793	0.512594
H-83	Brown amp-rich	3.8	962.1	0.011	0.703518	0.703479	14.81	86.2	0.1043	0.512745	0.512581
H-91	Brown amp-rich	9.5	913.7	0.030	0.703339	0.703236	13.65	75.8	0.1094	0.512766	0.512594
H-92	Brown amp-rich	8.9	949.8	0.027	0.703059	0.702966	13.88	76.2	0.1106	0.512694	0.512520
SY-6	Brown amp-rich	5.5	874	0.018	0.703491	0.703429	14.67	69.6	0.1280	0.512747	0.512546

[a]Assumes single-stage evolution, with depleted mantle (DM) = 0.513151, and 147/144 = 0.219.

The REE patterns (Figures 10b and 10d) are light REE enriched, with La_N/Yb_N (chondrite normalized) ranging from 11 to 26. Within petrographic groups, the REE data are tightly clustered, with coefficients of variation mostly <5%. The clinopyroxene gabbros have steeper patterns than the amphibole gabbros, and have lower Yb_N; all of the gabbros also have sloped REE patterns in the heavy REE (HREE; $Gd_N/Yb_N > 3$). There are no Eu anomalies, but some of the amphibole gabbros have slightly depleted Ce. The REE, particularly the HREE, distinguish the four petrographically identified sample groups, with HREE content increasing from the fine-grained clinopyroxene gabbros to the medium-grained clinopyroxene gabbros, to the brown and blue amphibole-bearing gabbros, to the brown amphibole-bearing gabbros.

5.3.3. Sr, Nd and Pb Isotopic Data

We report isotopic data for 15 samples (Table 2 and Figure 11). $^{87}Sr/^{86}Sr$ isotopic compositions are unradiogenic (< 0.705 at 240 Ma), with many samples having ratios lower than estimated bulk silicate earth (BSE). Rb/Sr and 1/Sr show no systematic relationship with $^{87}Sr/^{86}Sr$, but the amphibole gabbros have lower $^{87}Sr/^{86}Sr$ at 240 Ma than the clinopyroxene gabbros. $^{143}Nd/^{144}Nd$ isotopic compositions are between 0.51245 and 0.51260 at 240 Ma ($2.4 < \varepsilon_{Nd} < 5.2$), with $^{147}Sm/^{144}Nd$ between 0.099 and 0.128. Nd isotopic compositions show no systematic relationship with either $^{147}Sm/^{144}Nd$ or 1/Nd. Nd isotopic data for the clinopyroxene-rich gabbros are tightly clustered and are approximately within analytical uncertainty (± 0.00003) of each other. The amphibole-bearing gabbros show scatter outside of analytical uncertainty and have higher $^{143}Nd/^{144}Nd$ than the clinopyroxene gabbros. Pb isotopic data are radiogenic, with present-day $^{206}Pb/^{204}Pb > 20.1$ and $^{208}Pb/^{204}Pb > 39.7$. Pb isotopic compositions show no systematic relationships with $^{238}U/^{204}Pb$, $^{232}Th/^{204}Pb$, or 1/Pb. The $^{238}U/^{204}Pb$ (μ) and $^{232}Th/^{204}Pb$ ($\mu\kappa$) are very high (75–130 and 300–480, respectively). Pb isotopic data are scattered, and values for clinopyroxene and amphibole gabbros overlap. At 240 Ma, initial $^{206}Pb/^{204}Pb$ and $^{207}Pb/^{204}Pb$ values straddle the geochron with apparent μ between 8 and 8.5.

6. Discussion

6.1. Age Constraints

The primary uncertainty in our age determinations is whether the dated minerals are igneous phases, representing the age of magmatic activity, or metamorphic phases, in which case the dates reflect the age of metamorphism. Petrographic examination shows that most of the rocks have igneous cumulate textures, overprinted by brittle deformation and greenschist facies mineral assemblages (epidote-chlorite-carbonate, ± clinozoisite ± titanite ± actinolite). Original igneous phenocrysts are fractured and bent (e.g., Figures 5a, 5c, and 5d), with some replacement along margins and fractures. The brittle fracturing affects

Table 2 *(continued)*

Sample	eNd(T)	T_{DM}[a]	Pb	U	Th	$^{238}U/^{204}Pb$	$^{232}Th/^{238}U$	206/204	207/204	208/204	(206/204)i	(207/204)i	(208/204)i
						μ	k						
H-2	2.4	0.75	0.9	1.6	6.1	122.1	3.94	21.140	15.683	41.400	16.527	15.448	35.677
H-68	3.2	0.64	0.9	1.6	6.1	122.3	3.94	21.153	15.712	41.521	16.531	15.477	35.787
SY-2	2.8	0.72	1.2	1.5	5.8	84.0	4.00	20.459	15.601	40.502	17.283	15.439	36.507
SY-3	2.8	0.72	1.1	1.6	6.3	99.3	4.07	20.982	15.623	41.147	17.231	15.432	36.340
SY-4	2.8	0.72	0.9	1.3	5.9	98.3	4.69	20.867	15.629	41.069	17.151	15.439	35.580
SY-5	3.0	0.70	1.1	1.5	6.1	93.3	4.20	21.056	15.635	41.295	17.528	15.456	36.627
H-58	3.1	0.66	1.1	2.1	7.4	130.6	3.64	21.011	15.668	41.260	16.075	15.416	35.600
H-63	3.2	0.65	1.2	2	7.5	114.0	3.88	21.102	15.672	41.178	16.792	15.452	35.919
H-65	3.4	0.64	1.4	1.9	7.9	92.8	4.30	21.153	15.672	41.087	17.645	15.493	36.341
H-66	3.0	0.67	1.4	1.9	7.2	92.8	3.92	21.144	15.692	41.102	17.635	15.513	36.775
H-85	5.2	0.59	1.3	1.5	6.4	77.5	4.41	20.726	15.649	40.116	17.798	15.500	36.050
H-83	4.9	0.54	1.2	1.9	6.6	107.0	3.59	20.935	15.712	40.352	16.891	15.506	35.780
H-91	5.2	0.54	1.1	1.8	6.1	108.6	3.50	20.166	15.683	39.744	16.061	15.474	35.218
H-92	3.7	0.64	1.2	2	6.3	112.0	3.26	20.677	15.738	40.140	16.443	15.523	35.801
SY-6	4.2	0.68	1.4	1.6	6.1	76.8	3.94	20.755	15.672	40.165	17.851	15.524	36.562

clinopyroxene, which is undoubtedly igneous, as well as kaersutitic amphibole, and we interpret the kaersutitic amphibole also to be a primary, igneous phase. Thus, we interpret the amphibole ages as approximating the age of igneous crystallization. Amphiboles in samples AC 46 and H 84 have precise ages (uncertainties of ±1 and ± 0.92 Ma, respectively) and constrain the age of intrusion to the interval between 242 and 245 Ma. The absence of a plateau in the $^{39}Ar/^{40}Ar$ data for sample H 36 probably reflects the existence of two generations of amphibole in this sample, a kaersutitic brown amphibole and a riebeckitic blue amphibole, with the riebeckite rims on kaersutite (e.g., Figures 5g, 5p, and 6h) being somewhat younger. It is not clear whether riebeckitic amphibole is a late-magmatic phase or a metamorphic phase, but it commonly occurs as overgrowths that are in optical continuity with kaersutite.

The poorly constrained U/Pb titanite age for sample SY-2 (256 ± 23 Ma) overlaps the amphibole $^{39}Ar/^{40}Ar$ ages within uncertainty. Based on petrographic observations, titanite is likely to be a metamorphic breakdown product of igneous ilmenite and kaersutitic amphibole. All of these age estimates are closure ages for temperatures of ~ 500° (K-Ar in amphibole; Harrison, 1981) to 600 °C (U/Pb in titanite; Heaman & Parrish, 1991; Cherniak, 1993). There are poorly constrained U/Pb zircon ages, ranging from 137 to 258 Ma, on potentially correlative units in the Tokat Massif (Catlos et al., 2013). The images in Catlos et al. (2013) show that none of the zircons are euhedral, and we interpret these zircons as metamorphic. Nevertheless, the oldest ages are 258 ± 28 and 254 ± 16 Ma (Catlos et al., 2013, uncertainty as 2 σ), comparable to the titanite age of our sample SY-2 (256 ± 23 Ma), and this age range may be an upper limit for the intrusion age of the gabbros. Within uncertainty, these U-Pb ages overlap our more precise $^{39}Ar/^{40}Ar$ ages for the amphiboles. We prefer the amphibole ages, measured on igneous kaersutite, as the best estimate of the age of gabbro intrusion. The 200–220 Ma average ages in Catlos et al. (2013) are consistent with other estimates of the age of metamorphism in the Karakaya Complex (Okay et al., 2002; Okay & Monie, 1997). It is difficult to separate the age of igneous activity from the age of metamorphism, and to get robust ages for these rocks.

Younger, unmetamorphosed ultramafic intrusions (cumulate wehrlites and gabbros) also occur within the Tokat Massif and have been dated at 203.3 ± 4.9 Ma (Eyuboglu, Santosh, Bektaş, & Chung, 2011). The Th/U ratios of the dated zircons are consistent with a magmatic origin; these ultramafic rocks do not contain monazite, whose crystallization can modify the Th/U of coexisting zircon (Harley et al., 2007). Though the Karakaya Complex has been interpreted to extend, discontinuously, for ~ 2,000 km across all of northern Turkey, with the Tokat Massif being its eastern extension (Okay & Göncüoğlu, 2004; Şengör & Yılmaz, 1981), it is possible that it is diachronous and that ages measured in western Turkey cannot be extrapolated to the eastern Pontide exposures. It is also clear that there are two distinct generations of mafic-ultramafic rocks in the Tokat Massif, with the older generation showing the effects of metamorphism. Despite the uncertainties, our best estimate of the intrusion age of the metagabbros, 242–245 Ma, provides a useful constraint for tectonic reconstructions.

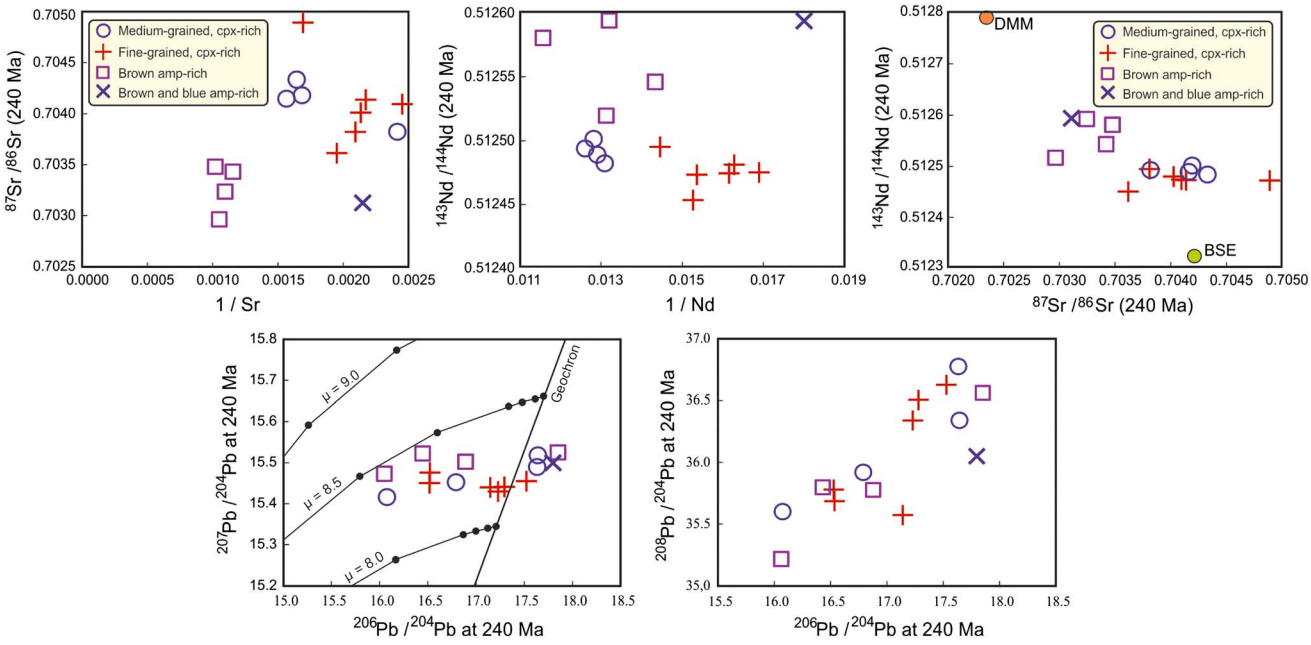

Figure 11. Plots of radiogenic isotopic data. (a) Initial $^{87}Sr/^{86}Sr$ shows no systematic relation with Sr concentration. The brown amphibole-rich gabbros are distinctive in having elevated Sr content with unradiogenic $^{87}Sr/^{86}Sr$. (b) Initial $^{143}Nd/^{144}Nd$ show no systematic relation with Nd concentration. The amphibole-rich gabbros are more depleted than the clinopyroxene gabbros. (c) Initial Sr and Nd isotopic compositions lie between depleted mantle (DMM) and estimated bulk silicate earth (BSE). Amphibole-rich gabbros show a higher percentage of the DMM component than the clinopyroxene gabbros. (d) Initial Pb isotopic compositions are consistent with derivation from a mantle source with $8 \leq \mu \leq 8.5$. There is no difference between amphibole-rich and clinopyroxene gabbros.

The occurrence, in fine-grained clinopyroxene-rich gabbros, of inherited zircons of several different ages is perplexing from a petrogenetic point of view. Inheritance is common in granitic rocks that are typically zircon saturated during much of their crystallization history (Watson & Harrison, 1983) but is less often observed in gabbroic rocks that are mostly zircon undersaturated. The inherited zircons indicate that the gabbroic magmas interacted with a range of crustal rock types during intrusion, and that crust much older than that exposed at the present surface existed along the intrusion path. This evident crustal history constrains the tectonic models that might be proposed for these rocks.

6.2. Petrogenetic Inferences

6.2.1. Effects of Metamorphism

The rocks included in this study contain two mineral assemblages—a primary igneous assemblage that includes clinopyroxene, kaersutitic amphibole, and opaque oxide phases and a greenschist facies metamorphic assemblage that includes actinolite, albite, calcite, chlorite, clinozoisite, epidote, and titanite; magmatic plagioclase has been completely replaced by metamorphic minerals. Blue, riebeckitic amphibole is either a late-magmatic phase or a metamorphic phase.

Sampling for this study was not directed toward the goal of determining how metamorphism has modified the bulk chemistry of the rocks. Thus, it is difficult to determine which features of the whole rock data are original igneous patterns, and which reflect metamorphism. Our starting assumption is that, for most elements, metamorphism has been isochemical on the hand sample scale. The most obvious exceptions to this generalization are the volatiles, H_2O and CO_2. The metamorphic or alteration assemblage (white mica, chlorite, epidote, clinozoisite, some titanite, and actinolitic amphibole) is hydrous and is consistent with the metamorphic grade of the rocks hosting the metagabbros (phyllites and greenschists). At the outcrop scale, carbonate veining indicates that CO_2 has been added to the rocks. It is not clear, however, whether the Ca associated with these veins is derived from breakdown of plagioclase—all analyzed plagioclase is albite (Figure 7)—or represents Ca addition during metamorphism. The persistent presence of both clinozoisite and epidote in the rocks suggests that Ca derived from breakdown of calcic plagioclase was primarily captured by these phases. Though diopsidic clinopyroxene can react with hydrous CO_2-rich fluids to produce tremolitic or actinolitic amphibole, the paucity of these amphiboles in the alteration assemblage, and the persistence of

Table 3
Pressures and Temperatures of Equilibration of Triassic Metagabbros

		P (kb)	*P* (kb) assumed	*T* (°C)	ΔFMQ	Equilibrium	Reference
H-20B	medium-grained, Cpx-rich	8.8		1205		Cpx-Bulk (hydrous)	1
		11.2		1219		Cpx-Bulk (hydrous)	2
		11.7		1258		Cpx-Bulk (anhydrous)	3
AC-41	medium-grained, Cpx-rich	11.3		1201		Cpx-Bulk (hydrous)	2
			11.3	555	3.03	Ilm-Mag	4
H-68	fine-grained, Cpx-rich	12.4		1234		Cpx-Bulk (hydrous)	2
		7.3		1047		Amp	5
H-85	blue and brown Amp rich	9.1		1058		Amp	5

Note. References: (1) Putirka (2008) equations (31) and (33): Jd-DiHd-EnFs formulations; (2) Putirka (2008) equation (32c) and (33): Al-partitioning (for *P*) and Jd-DiHd-EnFs (for *T*) formulations; (3) Putirka et al. (1996) equation (P1) and (T2); (4) Andersen and Lindsley (1988); (5) Ridolfi and Renzulli (2012). Core compositions of clinopyroxene and average compositions of kaersutite amphibole (brown core), ilmenite, and magnetite were used in the calculations.

relatively unaltered clinopyroxene in the pyroxene-rich gabbros, indicates that clinopyroxene was not a significant source of Ca during metamorphism. The variability of Ca in the whole rock analyses is large, compared with that of other major elements, and suggests that Ca and its proxies (light REE, Sr) may have been mobile on the hand-sample scale.

Sodium and the LILE, including K, Cs, Rb, Ba, and Pb, show scatter that is not systematic (Figures 10a and 10c). Their abundances are not related, for example, to the distribution of Al in a way that would be consistent with feldspars as their primary host minerals. The LILE therefore cannot be used as criteria for classification, and the Rb-Sr and U-Pb isotopic systems are potentially disturbed by LILE mobility. Disturbance of the Sm-Nd system has been documented in amphibolites (McCulloch & Black, 1984) and is typically associated with carbonate alteration and shearing. The rocks of the Tokat Massif do not show amphibolite grade metamorphism and are not strongly sheared but do have evidence of carbonate alteration, so that some disturbance of the Nd isotopic system cannot be excluded. Mobility of the LREE is indicated by the scatter of Ce in the brown and blue amphibole-bearing samples (Figure 10d). Riebeckitic amphibole has $Fe^{3+}/(Fe^{3+} + Al^{VI}) > 0.7$, implying that it is stable in oxidized environments; the mobility of Ce would be enhanced by oxidation of Ce^{3+} to Ce^{4+}.

6.2.2. Thermobarometry

Three of the four samples from which we collected mineral composition data are clinopyroxene-rich gabbros (H 68 is a fine-grained gabbro; AC-41 and H-20B are medium-grained gabbros); we have mineral composition data from one amphibole-rich sample, H-85, which contains both brown and blue amphiboles. Thermobarometric constraints calculated from the mineral data are shown in Table 3, as are the literature sources for the thermobarometric calibrations we used. We interpret the values calculated from clinopyroxene equilibria to be the temperatures (*T*) and pressures (*P*) of initial, igneous clinopyroxene crystallization, primarily because the clinopyroxene data used in these calculations are phenocryst core compositions. The estimated *P* ranges from 8.8 to 12.4 kb (~27- to ~40-km depth), with *T* exceeding 1200 °C. The estimates vary in detail, depending on whether hydrous or anhydrous compositions, are assumed for the bulk magma, but are consistent with experimentally observed liquidus conditions for clinopyroxene in basaltic magma compositions (e.g., Adam & Green, 1994). The uncertainty of the *T* estimates is generally <30 °C, whereas the uncertainty of the *P* estimates is ~ ± 3 kb. The *T* and *P* estimated from amphibole-bearing assemblages are somewhat lower (~ 1050 °C, and 7–9 kb) and are also consistent with experimentally observed conditions for the first crystallization of amphibole in hydrous basaltic compositions (e.g., Adam & Green, 1994; Gilbert et al., 1982). The amphibole equilibria were calculated with average compositions of the brown amphiboles, excluding the potentially metamorphic riebeckites. The *T* calculated from Ilm-Mt compositions clearly reflects postmagmatic conditions and is from phases that are not in equilibrium (igneous ilmenite and probably postmagmatic magnetite). None of the estimates constrain the P-T conditions of metamorphism because they are based on what we consider primary, igneous phases.

Our petrographic observations indicate that many of the clinopyroxene-rich gabbros are cumulates. The clinopyroxene exchange reactions used for *T* and *P* calculation assume equilibrium between clinopyroxene and a bulk rock composition that represents a magmatic liquid. The cumulate compositions are not liquid

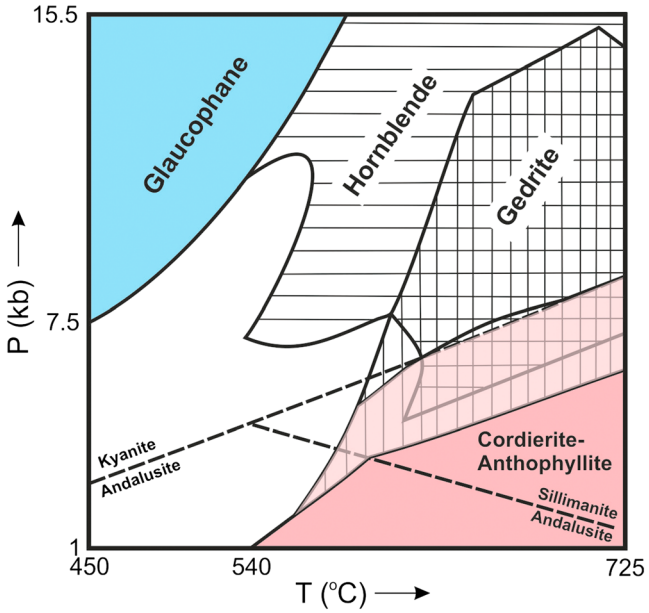

Figure 12. A schematic P-T diagram showing the approximate ranges of stability of blueschists (glaucophane-bearing) and cordierite-anthophyllite hornfels. The diagram, redrawn after Figure 6c in Diener et al. (2008), is anchored by the kyanite-sillimanite-andalusite triple point at ~4 kb and 550 °C. Other boundaries are approximate and depend on the compositions of the amphiboles that are present. The *P* limit of gedrite stability is at ~ 15.5 kb and 725 °C; the cordierite-anthophyllite assemblage intersects the 1 kb lower limit of the diagram at 540 °C.

compositions: there is therefore a fundamental uncertainty in the T and P estimates whose magnitude it is difficult to evaluate. Taken at face value, the clinopyroxene *T* and *P* data suggest initial crystallization near the base of the crust (~ 40 km).

Our data do not support the contention that the Tokat Massif was exposed to high-pressure, blueschist grade metamorphism during Early Triassic. There are two critical observations: first, the blue amphibole is riebeckite, not glaucophane (Figure 7), the characteristic mineral of the blueschist facies, and second, other minerals typical of the blueschist facies (lawsonite, aragonite) are absent, even though bulk rock compositions are in the range of their stability. The blue amphiboles we analyzed have high Fe^{3+}, unlike the low Fe^{3+} that is characteristic of glaucophane. No evidence of metamorphic conditions above greenschist grade has been found in the rocks of the Tokat Massif. Though blueschists and eclogites are reported within the Karakaya Complex in western Turkey (Okay et al., 2002; Okay & Göncüoğlu, 2004), the same conditions did not affect the eastern extension of the Karakaya Complex in the Eastern Pontides during the Early Triassic.

Additional constraints on the conditions of gabbro intrusion could be derived from the cordierite hornfels that occurs in the contact zone of the fine-grained clinopyroxene-rich intrusion in the extreme northeast corner of Figure 3, northeast of Ilyas. Other intrusions north of Ilyas also have hornfels zones, though poorly developed. This hornfels contains the assemblage cordierite (50%)-K-feldspar- plagioclase (15%)-quartz (10%)-anthophyllite (15%)-magnetite-hematite; cordierite, K-feldspar and plagioclase were identified by electron microprobe analyses. The absence of biotite is unusual. The coexistence of cordierite and K-feldspar implies a temperature, in the contact zone, in excess of 600 °C; this temperature is above that indicated by the greenschist facies regional metamorphic assemblage in the Tokat Massif rocks and confirms that the cordierite hornfels is a contact assemblage.

The pressure recorded by the contact assemblage is more difficult to constrain, in part because we have compositional data only on cordierite (Table S7), and in part because the assemblage in our samples lacks phases (Al silicates, garnet, orthopyroxene, spinel, and staurolite) that would help constrain pressure. Cordierite in the hornfels is relatively Fe-rich ($[Mg_{1.18}Fe_{0.78}]_{1.96}Al_{4.06}Si_{4.98}O_{18}$); average of nine analyses, Mg number ~ 60. No analyses of the anthophyllite are available; it is typically less magnesian than coexisting cordierite, and we expect the Mg number of anthophyllite to be 45–50. Rocks with a similar assemblage in the aureole of the Land's End granite in Cornwall (Pownall et al., 2012) are estimated to have reached peak *T* of ~ 615 °C, with P between 0 and 4 kb (most likely between 1 and 2.5 kb; Figure 27E of Pownall), and both of these estimates are compatible with the limited information we have about the rocks in the Amasya area. The hornfels *P* estimate is at least 4 kb below that derived from the clinopyroxene composition data and at least 3 kb below the *P* suggested by amphibole composition data, indicating that the gabbros were intruded to levels significantly shallower than the point of initial crystallization. Figure 12 is a schematic illustration of the *P-T* conditions under which blueschists (glaucophane-stable) and cordierite hornfels might form: the cordierite hornfels is a high-*T* low-*P* assemblage, whereas the blueschists are low-*T* and high-*P* rocks. Within the limits of our data on gabbros and host rocks, there is no evidence of metamorphic *P* exceeding 4 kb at the site of intrusion.

6.2.3. Igneous Petrology

Table 4 summarizes the geochemical data that serve to distinguish the four sample groups. Among the fine-grained clinopyroxene gabbros, four samples (SY-2, SY-3, SY-5, and H-2) have Mg numbers (molar $Mg/(Mg + Fe^{2+})$, where Fe^{2+} is calculated as 0.85 of total Fe) ≥ 68, indicating that they could have been magmas in equilibrium with peridotitic mantle. The Cr concentration (896–1,218 ppm) in these four samples is above that (~ 600 ppm) expected for magmas in equilibrium with peridotitic mantle, whereas their Ni content (88–153 ppm) is below the ~ 200 ppm expected of unfractionated melts from peridotitic mantle. The

Table 4
Summary of Compositional Features of Petrographic Groups

	Clinopyroxene gabbros		Amphibole gabbros	
	Fine grained	Medium grained	Brown and blue	Brown
SiO_2	40.52–42.99	41.22–42.76	42.75–43.83	43.41–46.01
Mg #	0.646–0.686	0.597–0.634	0.573–0.629	0.472–0.511
Al_2O_3	8.10–9.88	9.14–10.15	11.58–13.85	14.76–16.54
TiO_2	4.16–4.90	4.58–5.20	4.67–5.72	3.82–5.23
Na_2O	0.96–1.90	1.4–2.09	2.05–2.83	4.27–5.48
Ce	120–134	140–163	84–124	125–142
Cr	178–1218	137–390	<14–27	<14–14
Nb	65.0–84.7	85–104	50–75	77–86
Zr	310–357	350–416	334–414	426–479
$^{87}Sr/^{86}Sr(i)$	0.7036–0.7049	0.7038–0.7043	0.7031	0.7030–0.7035
e Nd (i)	2.4–3.2	3.0–3.4	5.2	3.7–5.2

trace element content, however, is consistent with clinopyroxene accumulation. The Mg number of clinopyroxene in the clinopyroxene gabbros is low (average 86), and only 9 of 69 analyses show Mg number > 90, the value expected of clinopyroxene in equilibrium with peridotitic mantle. Similarly, the maximum observed Cr_2O_3 content in clinopyroxene is 0.56 wt.%, below the ~1 wt.% that commonly occurs in clinopyroxenes in peridotitic mantle. The bulk rock molar Mg and Fe content of the clinopyroxene gabbros falls below the concentrations expected in unfractionated melts from peridotitic mantle (Hanson & Langmuir, 1978), but simple calculations show that <5 wt.% added Fo90 olivine would bring some bulk rock compositions into the field of peridotitic mantle melts and would also bring Ni content up to the range of mantle melts. These considerations, along with the petrographic observations of cumulate textures and the absence of olivine in the mode, indicate that the clinopyroxene gabbros are cumulate rocks formed primarily by clinopyroxene that crystallized from slightly fractionated magmas derived from melts of peridotitic mantle. Sample H-2 is the least fractionated composition.

By contrast, the Mg number of the other petrographically identified sample groups is consistently <64. The brown amphibole-rich gabbros have Mg number between 46 and 51, and despite their low SiO_2 (< 46 wt.%), are strongly fractionated, with no intermediate compositions that link them to the other sample groups. The Tokat Massif metagabbros thus represent rocks formed from variably fractionated magmas: they do not represent a continuous magmatic history. Indicators of the extent of fractionation are internally consistent, in that the brown amphibole-bearing gabbros have the highest SiO_2, Na_2O and incompatible trace elements (LREE, Zr, etc.), and the lowest Mg number and compatible trace elements (Cr and Ni). The only data that are not consistent with the inferred extent of fractionation are the Sr and Nd isotopic data. If all of the metagabbros derive from the same source, they should have isotopic compositions that are within analytical uncertainty, regardless of the extent of fractionation. But the more fractionated amphibole gabbros have lower $^{87}Sr/^{86}Sr$ and higher $^{143}Nd/^{144}Nd$ than the clinopyroxene gabbros, indicating either that the two gabbro types have different mantle sources, or that—counterintuitively—the clinopyroxene gabbros have been more contaminated by older crustal rocks than the more fractionated amphibole gabbros.

Geochemical data consistently show that the Tokat Massif metagabbros are alkaline (Figures 9a and 9b). Based on their normative compositions, three of the four petrographically identified sample types are silica undersaturated, with up to 11% normative nepheline; only the brown and blue amphibole-bearing samples are silica saturated (but not oversaturated). The gabbros plot in the alkaline gabbro field of a standard TAS diagram (Figure 9a), though some analyses plot at lower SiO_2 than the bounds of the conventional gabbro field. The trace element contents, particularly the HFSE (Ti, Zr, and Nb) and the REE are characteristic of alkaline, low-SiO_2 rocks, though Ti and Nb are elevated even compared with most alkaline rocks. Nevertheless, neither nepheline nor its alteration products were observed petrographically in any of the samples. There is no enrichment of the acmite component in the rims of clinopyroxenes, another feature common in alkaline gabbros. There is thus a mismatch between petrographic observations and the chemical indications that these are alkaline gabbros.

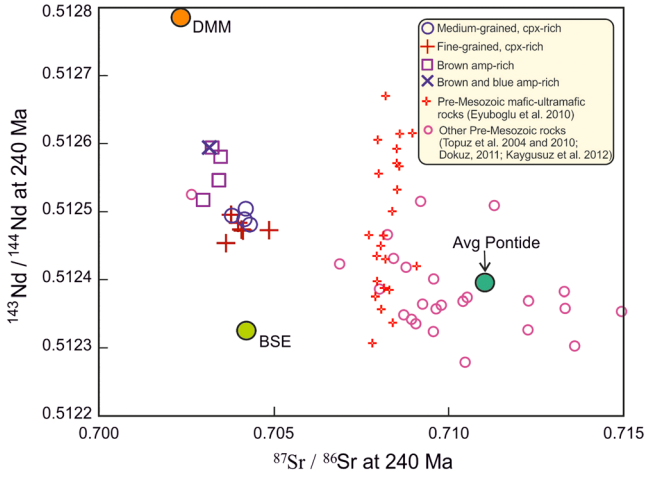

Figure 13. Initial Nd and Sr isotopic compositions of the Early Triassic gabbros are distinct from those of other pre-Mesozoic rocks in the Eastern Pontide Orogenic Belt, including the Late Triassic mafic-ultramafic rocks of the Pulur massif. Some analyses with elevated $^{87}Sr/^{86}Sr$ are excluded from this plot and from the calculated average of pre-Mesozoic igneous rocks. Data are from Dokuz (2011), Topuz et al. (2004, 2010), Eyuboglu et al. (2010) and Kaygusuz et al. (2012). DMM = depleted mantle; BSE = bulk silicate earth.

Only the brown amphibole-rich gabbros show exceptional enrichment of Na_2O; the enrichment of alkaline elements is not pronounced in the other sample groups. They plot in the alkaline gabbro field of the TAS diagram because of their exceptionally low SiO_2 content. The low SiO_2 and Al_2O_3 content is understandable in terms of the modal mineralogy of cumulate rocks consisting mostly of clinopyroxene or kaersutitic amphibole. To some extent, the enrichment of trace elements such as Zr and Nb can also be understood in terms of modal mineralogy, because clinopyroxene can host significant Zr, and Nb is commonly enriched in ilmenite, which is abundant in many of the gabbros. The source of this trace element enrichment is an open question.

Because the effects of metamorphism are not well constrained, the isotopic data, particularly for Sr and Pb, may not be reliable. The majority of the $^{87}Sr/^{86}Sr$ data are lower than BSE, and all of the $^{143}Nd/^{144}Nd$ plot between depleted mantle (DM) and BSE on a binary plot of the Sr and Nd systems (Figure 11). The Nd isotopic data are at odds with other geochemical data. The clinopyroxene gabbros are less fractionated than the amphibole gabbros, yet contrary to the patterns expected from assimilation-fractional crystallization models, their $^{143}Nd/^{144}Nd$ is lower than that of the amphibole gabbros. Though peridotitic mantle may be enriched at the time of melting, yielding trace element enriched alkaline magmas with isotopic compositions approximating that of DM, the low isotopic compositions of the clinopyroxene gabbros require either a source with long-term enrichment—a source that would no longer be peridotitic—or contamination with older crust, which is not very likely, given the high Mg number and low SiO_2 content of the rocks. Additionally, because of the high Nd content of the metagabbros, large degrees of crustal contamination would be required to shift the Nd isotopic composition, and both Mg number and SiO_2 content would reflect this contamination. Conversely, the higher $^{143}Nd/^{144}Nd$ of the amphibole gabbros implies less contamination or a less enriched source, but intermediate fractionation products are missing.

The Sr and Nd isotopic compositions of all Tokat samples lie between DM and the bulk of the data for pre-Triassic crustal rocks in the eastern Pontides (Figure 13) and superficially suggest that mantle-crust mixing is a possible explanation for the distribution of the Tokat data. The high Nd concentration of the rocks, however, cannot be explained with average crust and typical DM. The observation that initial Pb isotopic compositions are near the geochron with model μ between 8 and 8.5 (Figure 11) suggests that the enrichment event that increased μ and κ values, and ultimately also the present-day isotopic compositions, occurred close to the time of magma generation in the mantle.

DM model ages for the Nd isotopic data (T_{DM}), calculated assuming a single-stage evolution, range from 540 to 750 Ma (Table 2). This is ~300 Ma older than the best estimate of the age of magmatism and would suggest

that mantle enrichment could have occurred as much as 300–500 Ma before magmatism. The Pb isotopic data are not consistent with such an older enrichment event. The Nd T_{DM} estimates are, however, within the range of U-Pb ages measured on zircons in the fine-grained clinopyroxene gabbros (460–880 Ma); this may be a coincidence that reflects the poor constraints on both types of data, or it may hint at a role for older crust in the petrogenesis of these rocks. Thus, though isotopic data are most easily interpreted as indicating crustal contamination, there are inconsistencies between contamination models and both major and trace element abundances. The participation of enriched mantle is required by the combination of isotopic data and trace element abundances.

The multielement variation patterns (Figures 10a and 10c) of all Tokat sample groups are consistent with trace element enriched mantle sources. There is no hint in these data of an arc-like, or continental margin component: the HFSE are enriched, not depleted, and Pb, which typically is enriched in igneous rocks that have a continental crustal component, is strongly depleted. The simplest interpretation of these data is that the Tokat rocks are derived from magmas formed by low extents of melting in an enriched source that retained a dominantly peridotitic mineralogy. The clinopyroxene-rich gabbros have a clinopyroxene cumulate component, but the rocks overall represent low extents of crystallization of their parental magmas. The amphibole-rich gabbros derive from a source that is both isotopically distinct from and more hydrous than that of the clinopyroxene-rich gabbros.

Interpreting the igneous petrogenesis of the Tokat samples is difficult because they have few analogs. We have compared our data with other rocks of the Karakaya Complex (analyses from Catlos et al., 2013; Eyuboglu, Santosh, Bektaş, & Chung, 2011; Genç, 2004; Sayit & Göncüoğlu, 2009; Sayit et al., 2010). It is clear from Figure 14 that the clinopyroxene gabbros, with low SiO_2, Al_2O_3, and Na_2O, and high Fe_2O_3(t) and TiO_2 are unique among the Karakaya Complex rocks. Among the trace elements, HFSE (Nb and Zr) and LREE (Ce) are clearly distinctive in our samples, compatible trace elements like V are also elevated, but Sr and Yb overlap in part with data from other locations. In comparison with the cumulate rocks studied by Eyuboglu, Santosh, Bektaş, and Chung (2011), the cumulate-textured clinopyroxene gabbros show systematic enrichments in most trace elements. The geochemical differences between the Tokat and other Karakaya samples, the distinction in their apparent ages, and the differences in metamorphic histories suggest that the Tokat Massif may not be part of the Karakaya Complex.

Comparison with data extracted from the GeoRoc database also shows that the Tokat samples are unusual. The GeoRoc samples (GeoRoc, 2017; approx. 400 analyses; Figure 15) were selected to include those with SiO_2 between 40 and 46 wt. % and were further sorted by reported rock type. Thus, the *Al-rich* GeoRoc samples contain$>$18 wt. % Al_2O_3 and are anorthosites, anorthositic gabbros, and nepheline syenites; these do not compare with the low Al_2O_3 gabbros of this study. The *Other* samples plotted in Figure 15 include a broad range of rock types, including dunites, peridotites, pyroxenites, picrites, lamprophyres, and a range of alkaline basaltic rocks; among these, the MgO-rich peridotitic, picritic, and dunitic rocks are not relevant to interpretation of the Tokat gabbros. The main cluster of GeoRoc samples, plotted as *Gabbro* data, consists of gabbros, basalts, diabases, and unidentified rock types primarily from continental tholeiite provinces or large dike swarms (e.g., Emeishan in China and Franklin and the Mackenzie dikes in Canada). Few analyses from the GeoRoc database overlap the clinopyroxene gabbros in SiO_2-Al_2O_3 content, and even fewer match their high TiO_2 content. The more silicic and aluminous brown-and-blue amphibole gabbros have Na_2O that exceeds that found in any other rocks in this SiO_2 range. Among the trace elements, Nb, Zr, and Ce are again distinctive; V is elevated compared with other samples of similar MgO content; and Sr and Yb overlap concentrations measured in other basaltic compositions. The low SiO_2 content of the Tokat Massif samples does not overlap the range of the more silicic basaltic rocks from ocean island or continental rift settings, so that these two tectonic environments are not strongly represented among the selected GeoRoc data.

The basaltic igneous rocks of the Karakaya Complex, elsewhere in Turkey, have been ascribed to continental rift (Genç & Yılmaz, 1995; Koçyigit, 1987), ocean island (Çapan & Floyd, 1985; Sayit et al., 2010), or large igneous province (Genç, 2004) environments. None of the prior studies of the Karakaya Complex are supported by isotopic analyses. Though there are some features that compare well with each environment, there are other indicators that make each association difficult. The Tokat Massif samples are distinct from the other Karakaya rocks, so they probably do not share the petrogenetic history of other Karakaya samples. The small volume of the preserved materials suggests that association with a large igneous province is unlikely. Though

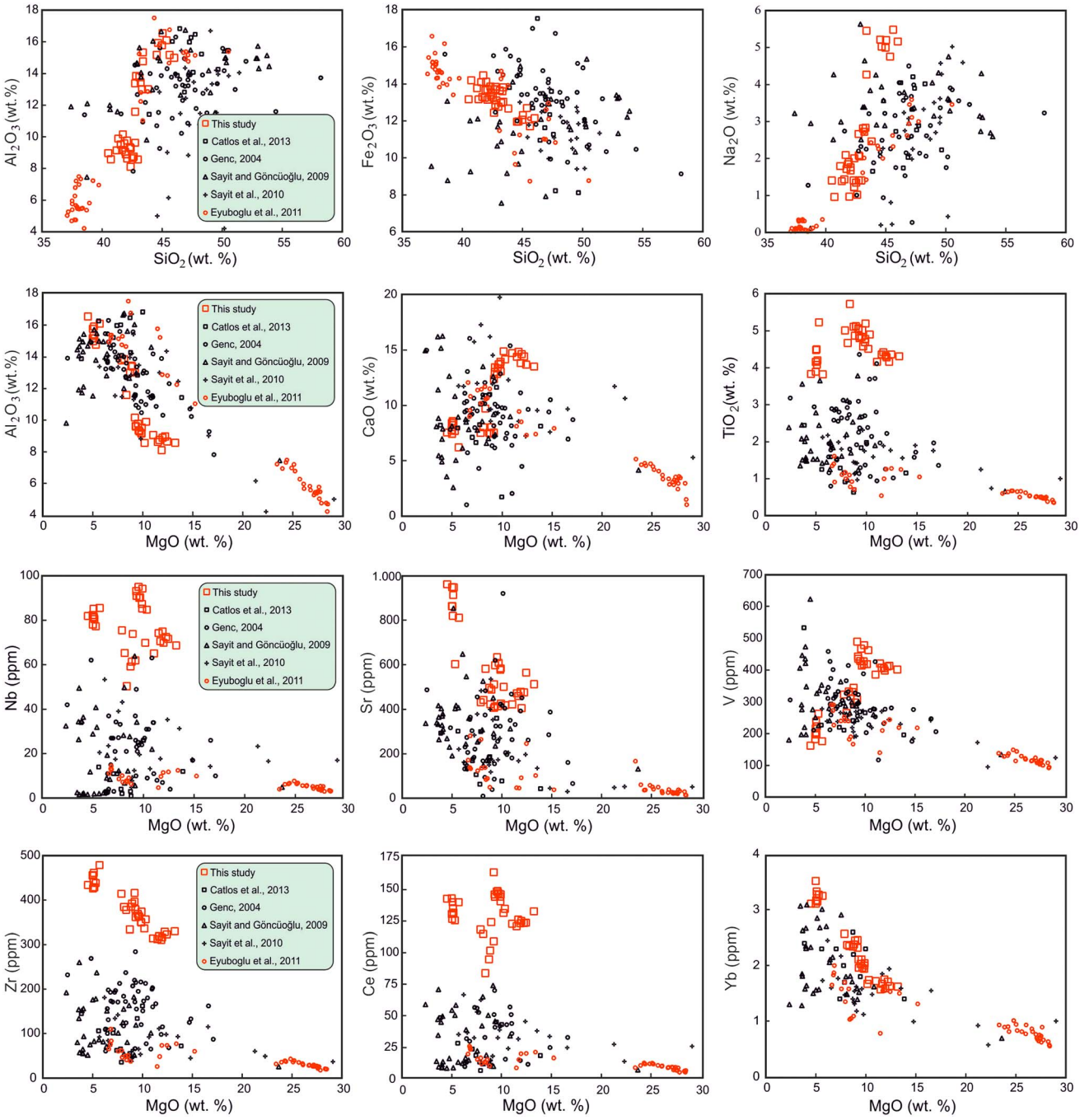

Figure 14. Bivariate variation diagrams that compare data from this study with analyses of metabasalts, metadiabases, and metagabbros included in the Karakaya Complex show that the alkaline gabbros of this study are distinct from other Karakaya lithologies. Especially notable are the elevated TiO_2, Ce, Nb, and Zr of the alkaline gabbros. Data from Catlos et al. (2013), Eyuboglu, Santosh, Bektaş, & Chung (2011), Genç (2004), Sayit and Göncüoğlu (2009), and Sayit et al. (2010).

there is evidence of an enriched mantle source, there is no evidence of arc-associated enrichment (high LREE and Ba, low HFSE), and SiO_2-poor arc rocks typically have shallower sources ($<$ 25 km). Among ocean island basalts, alkaline compositions are usually volumetrically minor, occur late in the eruption sequence, and overlie the dominant tholeiitic rocks; the absence of typically tholeiitic rocks makes it difficult to associate these with an ocean island source, even though the multielement variation diagrams are similar to those of many OIB**.** Many continental rifts have a bimodal volcanic suite, but others, like the Central Atlantic Magmatic Province in eastern North America, have little associated felsic magmatism. The presence of

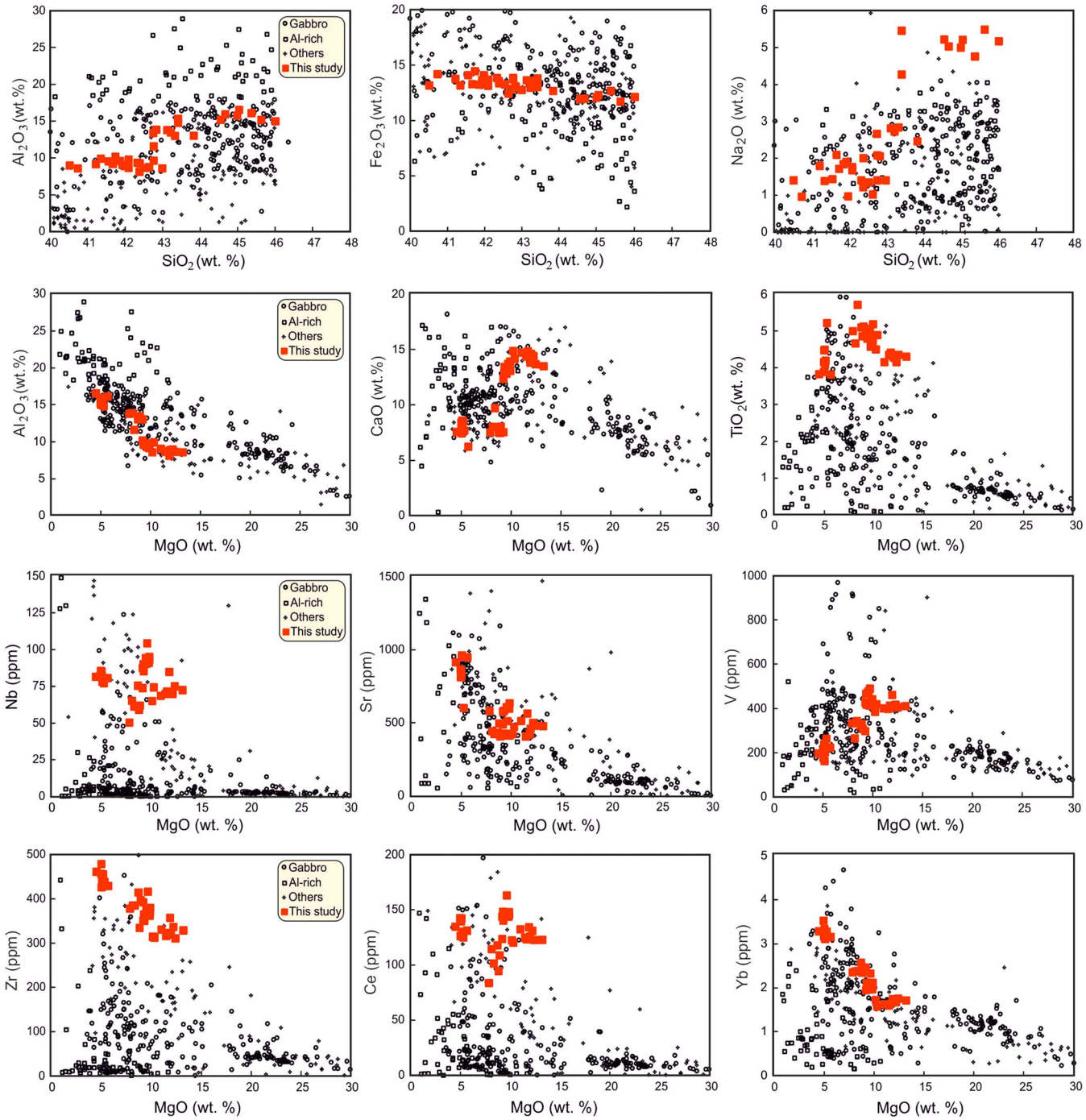

Figure 15. Bivariate variation diagrams show alkaline gabbros of this study with analyses selected from the GeoRoc database based on comparable major element content (see text). Only a small fraction of analyses in the literature match the alkaline gabbros in TiO_2, Ce, Nb, and Zr content.

inherited, older zircons in some of the clinopyroxene gabbros and the depth of initial clinopyroxene crystallization at ~ 40 km is consistent with the formation of these rocks in a continent-associated setting.

6.3. Tectonic Inferences

Among scientists who focus on geodynamic evolution of the Alpine-Himalayan system, the Permo-Triassic geographic position of the Pontides Orogenic Belt is still being discussed. Some researchers believe that the Pontides Orogenic Belt during the Permo-Triassic was the southern margin of Laurasia (e.g., Adamia

et al., 1977, 1981; Okay & Nikishin, 2015; Okay & Tüysüz, 1999). In this model, the Black Sea represents a Cretaceous back-arc basin that opened north of the Pontides Orogenic Belt during northward subduction of Tethys oceanic lithosphere. In contrast, Dewey et al. (1973) suggested that the Pontides Orogenic Belt belongs to Godwana and that its geodynamic evolution is related to southward subduction of Paleo-Tethyan oceanic lithosphere that was located north of the belt during the Late Paleozoic, Mesozoic, and Early Cenozoic. They also emphasized that the Black and Caspian Seas are remnants of the Tethys Ocean and interpreted the ophiolitic rocks exposed along the southern edge of the belt as remnants of a marginal basin behind Pontides Orogenic Belt. Aspects of this model for the Paleozoic to Miocene geodynamic evolution of northern Turkey were subsequently supported by many researchers (e.g., Akaryalı, 2016; Bektaş, 1981; Bektaş et al., 1999; Eyuboglu, 2010, 2015; Eyuboglu et al., 2007, 2012, 2014, 2018; Eyuboglu, Chung, et al., 2011; Eyuboglu, Dudas, et al., 2013; Eyuboglu, Dudas, Santosh, Xiao, et al., 2016; Eyuboglu, Dudas, Santosh, Zhu, et al., 2016; Eyuboglu, Santosh, Bektaş, & Chung, 2011; Eyuboglu, Santosh, & Chung, 2011; Eyuboglu, Santosh, Dudas, et al., 2011; Maden, 2013; Maden et al., 2009).

Şengör and Yılmaz (1981), consistently with the Dewey et al. (1973) model of southward subduction, assigned the Pontides Orogenic Belt to Gondwana during Permo-Triassic time. They proposed, however, that in the Early Jurassic a new ocean, the Northern Branch of Neotethys, opened as a back-arc basin and closed by northward subduction under the Pontide arc during the Late Mesozoic, followed by subsequent collision between the Tauride and Pontide blocks in the Early Cenozoic. They interpreted the mafic-ultramafic lithologies in the south of the Pontides Orogenic Belt as a Penrose-type ophiolite sequence, remnants of Jurassic ocean ridge lithosphere of the Northern Branch of Neotethys. However, recent systematic geological, geochemical and geochronological studies do not support this proposal for Jurassic to Cenozoic geodynamic evolution of northern Turkey. Eyuboglu, Dudas, Santosh, Xiao, et al. (2016) obtained crystallization ages ranging from Silurian to Jurassic for mafic intrusions within the Kop ultramafic massif, indicating that at least some of the serpentinized ultramafic rocks in the south of the orogenic belt are Paleozoic and cannot be remnants of Jurassic oceanic crust as suggested by Şengör and Yılmaz (1981).

Most Permo-Triassic rocks exposed in the Pontides Orogenic Belt are assigned to the Karakaya Complex that has played a key role in interpreting the Permo-Triassic geodynamic evolution of northern Turkey. This unit is generally divided into two subunits (Koçyigit, 1987). The Lower Karakaya Complex, known widely as the Nilüfer Unit (Okay et al., 1991), consists mainly of metabasites intercalated with phyllite and marble that have undergone greenschist and blueschist facies conditions during the Late Paleozoic or Triassic. The Upper Karakaya Complex includes mainly clastic, volcaniclastic and volcanic rocks (e.g., Okay et al., 1991, 2002; Okay & Göncüoğlu, 2004).

There are two main hypotheses for the origin of the Karakaya Complex. Some authors suggested that it was deposited in a rift that opened as a marginal sea in the Late Permian-Early Triassic, as a result of southward subduction of Paleo-Tethyan oceanic lithosphere. This rift basin would have closed in Late Triasssic-Early Jurassic time (e.g., Bingöl et al., 1975; Genç & Yılmaz, 1995; Göncüoğlu et al., 2000; Koçyigit, 1987; Sayit et al., 2010; Şengör & Yılmaz, 1981). According to this hypothesis, Paleozoic limestone blocks in the upper part of the sequence are derived from the rift shoulders. Conversely, some workers consider the Karakaya Complex to be a subduction-accretionary complex related to northward subduction of oceanic slab(s) during the Late Permian-Triassic (e.g., Catlos et al., 2013; Okay, 2000; Pickett & Robertson, 1996; Pickett & Robertson, 2004; Tekeli, 1981). Some researchers (e.g., Okay & Göncüoğlu, 2004; Pickett & Robertson, 2004; Robertson & Ustaömer, 2012) suggested that the mafic crustal material of the Nilüfer Unit (Lower Karakaya Complex) formed in oceanic islands or an oceanic plateau in Permo-Triassic time (Catlos et al., 2013; Genç, 2004; Okay, 2000; Sayit & Göncüoğlu, 2013) and was accreted to the southern margin of Laurasia in Late Triassic time as a result of northward subduction of Tethys oceanic lithosphere.The Eastern Pontides Orogenic Belt contains several metamorphic massifs (Pulur, Ağvanis, and Tokat), as well as smaller outcrops of metamorphic rocks (Kurtoğlu, Beyçam, Petekkaya, Kopuzsuyu, Kop Mountain, Karadağ, and Dereli; Figure 2). Some workers suggest that the Karakaya Complex is not restricted to the western part of the Pontides Orogenic Belt and includes also the large metamorphic massifs of the Eastern Pontides Orogenic Belt, excepting only the high-grade part of the Pulur massif (e.g., Genç, 2004; Okay, 1996; Okay & Göncüoğlu, 2004; Yılmaz & Yılmaz, 2004).

Topuz et al. (2014) suggested that Ağvanis metamorphic massif represents an oceanic accretionary complex depending on the geochemical characteristics of metabasites,that reveal island arc, mid-ocean ridge, and ocean island affinities, and it can be correlated with the Nilüfer unit of Karakaya Complex in the western part of Pontides. However, some studies clearly indicated that the geochemical diversity of the basaltic lithologies in the same location is not unique for the oceanic settings and/or forearc regions and may also implies a back-arc basin geodynamic setting (e.g., Smedley, 1986; Eyuboglu et al., 2007). In addition, Ağvanis metamorphic massif includes matadacites, which are intercalated with metabasic rocks, phyllites and thickly bedded marbles (Okay, 1984), supporting a bimodal activity and back-arc rift setting during the formation of their protoliths. Topuz et al. (2014) also emphasized that Ağvanis metamorphic massif underwent greenschist-albite-epidote-amphibolite-facies regional metamorphism at ~209 Ma. However, the age data obtained from some igneous lithologies exposed immediately northeast of Ağvanis metamorphic massif indicate that the timing of the regional metamorphism should be older than 209 Ma. The zircons extracted from unmetamorphosed porphyritic and volcanic rocks, which are exposed in 35 km northeast of Ağvanis metamophic massif and exhibit typical characteristics of subduction-related magmas, yielded U-Pb ages ranging from 203 to 218 Ma. Similarly, Karslı et al. (2014) reported an Ar/Ar cooling age of 216 Ma from unmetamorphosed lamprophyries exposed in the same region.

In a comprehensive study focusing on the geology and structural evolution of the Tokat Massif, Yılmaz et al. (1997) classified the massif's lithologies into three groups: (i) The Yeşilırmak Group, belonging to Gondwana, consists of a Paleozoic metamorphic core that displays polyphase metamorphism reaching amphibolite facies, and an overlying Triassic sequence that has undergone regional dynamothermal metamorphism during the Late Triassic; (ii) the Turhal Metaophiolite that tectonically overlies the Yeşilırmak Group and has undergone greenschist facies metamorphism; and (iii) the Amasya Group that is represented by a Lower Paleozoic clastic sequence including mineral assemblages at greenschist facies. Thus, the highest metamorphic grade in the Tokat Massif is amphibolite, and there are pre-Triassic, Paleozoic units that show only greenschist grade assemblages. If the Tokat Massif includes units that correlate with the Karakaya Complex, these have not been exposed to high-*P*, low-*T* metamorphism.

Our detailed geological, petrographical, geochemical, and chronological studies on the intrusive bodies cutting the low-grade metamorphic lithologies of the Tokat Massif indicate that there are at least two different types of pre-Jurassic ultramafic-mafic intrusions in the Amasya region. These are (i) Late Triassic wehrlite and gabbro intrusions (Eyuboglu, Santosh, Bektaş, & Chung, 2011) and (ii) Early Triassic gabbro intrusions (this study). The geochemical characteristics of both groups of mafic-ultramafic intrusions are inconsistent with those of igneous lithologies reported from the Karakaya Complex (Eyuboglu, Santosh, Bektaş, & Chung, 2011, and this study).

The Late Triassic wehrlite and gabbro bodies occur as small discordant intrusions within the low-grade metamorphic lithologies of the Tokat Massif (Figure 3). They have the petrographic and geochemical characteristics of Alaskan-type intrusions, presumably derived from a subduction-related, high-alumina, hydrous basaltic parental magma in a convergent plate setting (Eyuboglu, Santosh, Bektaş, & Chung, 2011).

The second type of mafic intrusions, the Early Triassic alkaline metagabbros, consist mainly of clinopyroxene, both brown and blue amphibole, and plagioclase. The ^{40}Ar-^{39}Ar dating of magmatic amphiboles clearly indicates that the alkaline gabbros were emplaced into low-grade metamorphic lithologies of the Tokat Massif during the Early Triassic. The identification of blue amphiboles in Pre-Jurassic gabbros in the Amasya region has contributed to development of models for the geodynamic evolution of northern Turkey, and also to interpretation of metamorphic conditions in the Tokat Massif. Rojay and Göncüoğlu (1997) emphasized that the protoliths of low-grade metamorphic rocks in the Amasya region were an arc-related basinal sequence that was first subjected to regional dynamothermal metamorphism in the late Paleozoic, with a later, Early Mesozoic (?), high-pressure/low-temperature metamorphism that produced the Na-amphibole overgrowths. Catlos et al. (2013) divided metagabbros exposed in the Amasya region into two groups, one belonging to the Karakaya Complex and the other to Neo-Tethyan crust. Without mineral chemistry data, they identified the blue, secondary amphiboles in two Karakaya gabbros (AT25B and AT-23A) as glaucophane and proposed that these gabbros have undergone subduction-related blueschist metamorphism. Catlos et al. (2013) stated that glaucophanes in sample

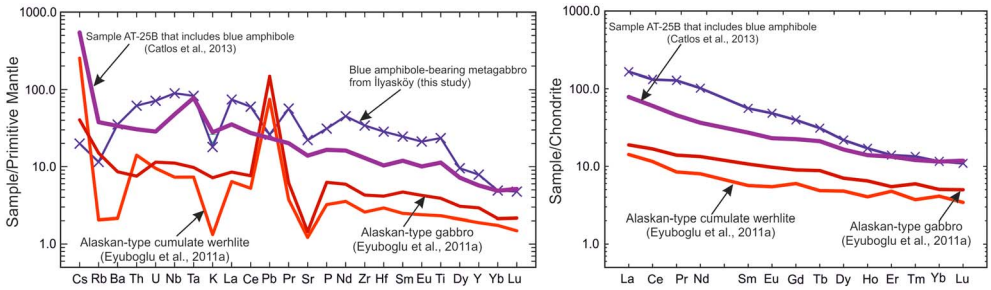

Figure 16. Primitive mantle-normalized trace (left) and chondrite-normalized rare earth element (right) distribution patterns for the mafic lithologies cutting Tokat Massif in the Amasya region (primitive mantle values: Sun & McDonough, 1989; chondrite values: Boynton, 1984).

AT23A occur as rims on brown amphiboles. This petrographic characteristic is consistent with our observations on blue amphibole-bearing alkaline gabbros. Sample AT25B is chemically similar to the alkaline gabbros presented in this study, with high Na_2O (4.05 wt.%), TiO_2 (2.44 wt.%), Zr (145 ppm), and Nb (34 ppm) content, and similar trace element and REE distributions (Figure 16). Catlos et al. (2013) linked the pre-Jurassic lithologies in the Amasya area to the Karakaya Complex, which includes igneous rocks that may have been produced in seamount, mantle plume, and MOR-related settings of the Paleotethys. The Complex itself is interpreted to be a subduction-accretion system formed in the Late Triassic, in which these pieces of the Paleotethys oceanic realm were joined and incorporated. However, our study of these blue amphibole-bearing alkaline metagabbros clearly indicates that they should not be included in the Karakaya Complex and have not undergone blueschist metamorphism. Their major and trace element and REE concentrations are distinct from the other Karakaya rocks (Genç, 2004; Sayit & Göncüoğlu, 2013), so they do not share the petrogenetic history of other Karakaya samples (Figures 14 and 15). The microchemical studies on the blue amphiboles clearly indicate that they are magnesioriebeckite, not glaucophane. In addition, the presence of epidote, albite, titanite, and preferentially aligned chlorite and mica that wrap around larger crystals indicate low-grade metamorphism of these samples. An estimate of the metamorphic conditions using the magnesioriebeckite compositions and the barometer of Anderson and Smith (1995) yields negative pressures at all temperatures below 1200 °C. Thus, metamorphism may have happened at shallow depths during exhumation of the gabbroic bodies, or during regional metamorphism.

Continental rift zones are characterized by bimodal igneous lithologies and immature terrigenous clastic sediments (Wilson, 1993), though some rift environments—the circa 200 Ma Central Atlantic Magmatic Province exposed in the eastern United States, for example—have few or no felsic igneous rocks. This study documents Early Triassic, nepheline-normative, clinopyroxene- and kaersutite-rich alkaline gabbro magmatism in the Amasya area. In his study of the geology and stratigraphy of the Amasya area, Alp (1972) reported Na-rich syenites (albite, amphibole, and chloritized biotite), and alkaline syenite pegmatites (mainly albite and chlorite), which may be the felsic components of bimodal magmatism in the study area during the Pre-Jurassic time.

The study area is mainly underlain by schists and phyllites that are the westward extension of the Tokat Massif that extends for almost 200 km in the southwestern part of the Eastern Pontides Orogenic Belt (Figures 2 and 3). These metamorphic units are unconformably overlain by the Karasenir formation that consists mainly of partly and/or weakly metamorphosed terrigenous sedimentary rocks, including lenticular limestone bodies which are fossiliferous and yield a Silurian age (Alp, 1972). However, Yılmaz et al. (1997) suggested that the Amasya metamorphic association (Alp's, 1972, Karasenir Formation) occurs as a nappe that rests tectonically on the upper units of the Tokat Massif. According to Çapkınoğlu and Bektaş (1997), the limestone bodies are olistoliths within the Karasenir Formation; some contain Early Devonian conodonts and Permian algae. Based on the fossil evidence, they suggested that the Karasenir Formation belongs to the Triassic Karakaya Complex, the uppermost section of which is exposed around Amasya. Eyuboglu (2006) also suggested that low-grade metamorphic lithologies of the Tokat Metamorphic Massif are unconformably overlain by Triassic terrigenous sedimentary rocks, mainly arkosic sandstones with angular to subangular quartz (40–60%) and plagioclase (10–20%) along with fragments

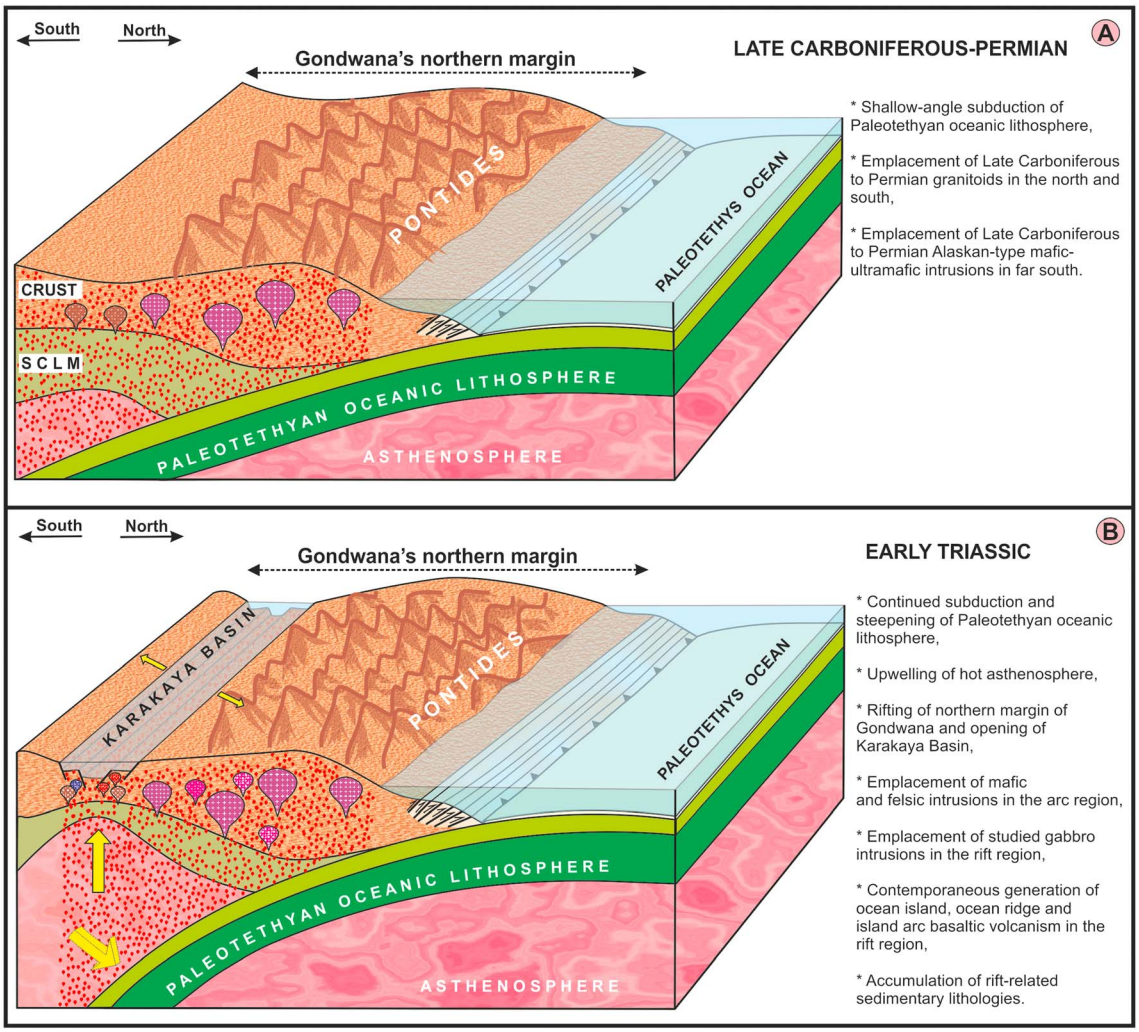

Figure 17. Cartoon showing the Late Paleozoic to Early Triassic geodynamic evolution of Gondwana's northern margin and the formation of the studied alkaline metagabbroic rocks. (a) Long-lived, gently south dipping subduction of Paleotethyan oceanic lithosphere and the emplacement of granitoids in arc and Alaskan-type mafic-ultramafic intrusions in the backarc. (b) Steepening of the southward subducting lithosphere, opening of the Karakaya Basin south of the Pontides Belt, and simultaneous emplacement of alkaline gabbros into thinned continental crust.

of low-grade metamorphic rocks (10–20%). Eyuboglu (2006) emphasized that this sedimentary sequence, including the exotic limestone blocks, accumulated in a rift-related setting in Triassic time. These pre-Jurassic units are disconformably overlain by the Early to Middle Jurassic Kayabaşı Formation of nonmetamorphic terrigenous sedimentary rocks.

6.4. The Late Paleozoic-Early Mesozoic Tectonomagmatic Evolution of Northern Turkey

Throughout the Pontides belt, Late Paleozoic time is characterized by intense felsic plutonic activity. Published geochronological data from granitoids exposed in both the northern and southern parts of the Eastern Pontides Orogenic Belt indicate that they were emplaced into metamorphosed crustal rocks between 348 and 300 Ma (e.g., Dokuz, 2011; Kaygusuz et al., 2012, 2016; Topuz et al., 2010). However, our geochronological data from granitoids exposed in the Artvin and İspir areas in the eastern part of the orogenic belt suggest that this felsic plutonism continued until circa 264 Ma (Guadalupian). In the far south part of the orogenic belt, the same time span is represented by Alaskan-type mafic-ultramafic intrusions whose source is interpreted to be subcontinental lithospheric mantle that was metasomatized during the subduction of Paleotethyan oceanic lithosphere (Eyuboglu et al., 2010; Eyuboglu, Dudas, Santosh, Xiao, et al., 2016). Late Paleozoic granitoids are also widespread in the central and western Pontides, with ages clustered between

320 and 250 Ma (e.g., Gücer et al., 2016; Nzegge et al., 2006; Okay et al., 2015; Okay & Topuz, 2017; Şahin et al., 2012; Sunal et al., 2006).

The prevailing interpretation is that the Late Paleozoic granitoids were formed in a subduction-related setting, but the subduction polarity remains unclear. Conversely, Dokuz (2011) and Kaygusuz et al. (2016) suggested that the Late Paleozoic granitoids of the Eastern Pontides Orogenic Belt formed during the collision of the Laurasia and Gondwana plates following the closing of the Paleotethys Ocean. However, this scenario is not consistent with models of the life span of the Paleotethys Ocean that started to open in the Cambrian and closed in the Late Triassic (e.g., Golonka et al., 2018), Early Jurassic (e.g., Şengör & Yılmaz, 1981), or Cenozoic (e.g., Dewey et al., 1973).

Uyeda and Kanamori (1979) distinguished two types of subduction zones that differ in the dip of the downgoing plate. Mariana-type subduction zones have steeply dipping, old, relatively cool and therefore dense oceanic lithosphere leading to formation of deep trenches and opening of back-arc basins due to high extensional stress. Conversely, Chilean- or Andean-type subduction zones are characterized by gently dipping, younger, hotter and less dense oceanic lithosphere leading to formation of shallow trenches and crustal thickening due to high compressional stress. Chilean-type subduction settings typically have granitoids emplaced along large magmatic arcs thousands of kilometers long (e.g., Aguirre, 1983; Atherton & Petford, 1996; Bustamante et al., 2016; Hervé et al., 1988, 2007; Parada, 1990; Parada et al., 1999).

Considering all data, we suggest that the Late Paleozoic granitoids and Alaskan-type mafic-ultramafic intrusions were emplaced into crustal rocks of the Pontides Belt during prolonged, gently south dipping subduction of Paleotethyan oceanic lithosphere (Figure 17a). In the Early Triassic, steepening of the southward subducting lithosphere created an extensional setting that triggered opening of the Karakaya Basin south of the Pontides Belt (Figure 17b) and resulted in emplacement of alkaline gabbros into thinned continental crust. The gabbros show geochemical evidence of interaction with crustal rocks, of derivation from DM, and no indication of arc-related petrogenetic processes; we interpret them as remnants of an incipient back-arc rift in a continental block. This scenario also explains the diversity of basaltic lithologies reported from Karakaya Basin, including the preponderance of lavas in the western and central Pontides (Genç, 2004; Sayit et al., 2010; Sayit & Göncüoğlu, 2009), where the Triassic sequence is better preserved, and where the rifting may have progressed further than it did in the Amasya area.

7. Conclusions

The clinopyroxene-rich and amphibole-rich gabbros have different petrogenetic histories. All can be considered alkaline gabbros. Both derive from trace element enriched mantle. Both derive from magmas generated by low degrees of partial melting, and reflect relatively little fractional crystallization. The clinopyroxene-rich gabbros are partially clinopyroxene cumulates, reflect a mantle source with approximately peridotitic mineralogy, and have less fractionated Mg numbers than the amphibole-rich gabbros. The amphibole-rich gabbros contain magmatic, kaersutitic amphibole and derive from a source more hydrous than the source of the clinopyroxene-rich gabbros.

The blue amphiboles are magnesioriebeckites that formed either during metamorphism or during late-stage igneous crystallization. There is no evidence in the gabbros of a high-pressure metamorphic event. Clinopyroxene in the clinopyroxene-rich gabbros indicates that crystallization of the magmas began at ~40-km depth, at T near 1200 °C, whereas mineral compositions in the amphibole-rich gabbros indicate shallower and cooler crystallization conditions.

The Nd and Sr isotopic compositions of the amphibole-rich gabbros are closer to those of DM than those of the clinopyroxene gabbros, a feature that contrasts with the less fractionated composition of the clinopyroxene gabbros. This contrast most clearly indicates that the clinopyroxene and amphibole gabbros derive from distinct mantle sources.

The gabbros that cut the Tokat Massif are compositionally distinct from mafic igneous rocks in the approximately contemporaneous Karakaya Complex that is exposed in other parts of Turkey. Because of their low SiO_2 and Al_2O_3, and enriched TiO_2, Ce, Nd, and Zr, they also have few analogs among other gabbros reported in the literature. The gabbros are best interpreted as small volume magmas generated in an incipient back-arc rift that developed in pre-Mesozoic crust on the northern margin of Gondwana.

Acknowledgments
This project was supported by Karadeniz Technical University Research Foundation (grants 8980 and 5571). We thank John W. Geissman, Editor-in-Chief, and Mustapha Meghraoui, Associate Editor, for their constructive comments. We are grateful to Erdin Bozkurt and three anonymous reviewers for their valuable comments and suggestions, which improved the manuscript. We specially thank Gilles Ruffet for his help in $^{40}Ar/^{39}Ar$ dating of sample AC-46. We would also like to thank Kemal Akdağ for his helpful suggestions. Onur Akan, Ömer Boz, and Enver Akaryalı are thanked for their assistance with the fieldwork. The data used in this study are listed in the references, tables, and supporting information.

References

Adam, J., & Green, T. H. (1994). The effects of pressure and temperature on the partitioning of Ti, Sr and REE between amphibole, clinopyroxene and basanitic melts. *Chemical Geology*, *117*(1-4), 219–233. https://doi.org/10.1016/0009-2541(94)90129-5

Adamia, S. A., Chkhotua, T., Kekelia, M., Lordkipanidze, M. B., Shavishvili, I., & Zakariadze, G. (1981). Tectonics of the Caucasus and adjoining regions—Implications for the evolution of the Tethys Ocean. *Journal of Structural Geology*, *3*(4), 437–447. https://doi.org/10.1016/0191-8141(81)90043-2

Adamia, S. A., Lordkipanidze, M. B., & Zakariadze, G. S. (1977). Evolution of an active continental margin as exemplified by the Alpine history of the Caucasus. *Tectonophysics*, *40*(3-4), 183–199. https://doi.org/10.1016/0040-1951(77)90065-8

Ağar, Ü. (1977). Demirözü (Bayburt) ve Köse (Kelkit) bölgesinin jeolojisi (Doctoral dissertion). İstanbul Üniversitesi Fen Fakültesi, 55 pp (in Turkish with English abstract).

Aguirre, L. (1983). Granitoids in Chile. *Geological Society of America Memoirs*, *159*, 293–316. https://doi.org/10.1130/MEM159-p293

Akaryalı, E. (2016). Geochemical, fluid inclusion and isotopic (O, H and S) constraints on the origin of Pb–Zn ± Au vein-type mineralizations in the Eastern Pontides Orogenic Belt (NE Turkey). *Ore Geology Reviews*, *74*, 1–14. https://doi.org/10.1016/j.oregeorev.2015.11.013

Alp, D. (1972). Geology of the Amasya region (Doctoral dissertion). İstanbul Üniversitesi Fen Fakültesi Monografileri, 101 pp (in Turkish with English abstract).

Andersen, D. J., & Lindsley, D. H. (1988). Internally consistent solution models for Fe-Mg-Mn-Ti oxides: Fe-Ti oxides. *American Mineralogist*, *73*, 714–726.

Anderson, J. L., & Smith, D. R. (1995). The effect of temperature and oxygen fugacity on Al-in-hornblende barometry. *American Mineralogist*, *80*(5-6), 549–559. https://doi.org/10.2138/am-1995-5-614

Armstrong, J. T. (1995). CITZAF-A package for correction programs for the quantitative electron microbeam X-ray analysis of thick polished materials, thin-films and particles. *Microbeam Analysis*, *4*, 177–200.

Arslan, M., & Aslan, Z. (2006). Mineralogy, petrography and whole-rock geochemistry of the Tertiary Granitic Intrusions in the Eastern Pontides, Turkey. *Journal of Asian Earth Sciences*, *27*(2), 177–193. https://doi.org/10.1016/j.jseaes.2005.03.002

Atherton, M. P., & Petford, N. (1996). Plutonism and the growth of Andean Crust at 9°S from 100 to 3 Ma. *Journal of South American Earth Sciences*, *9*(1–2), 1–9. https://doi.org/10.1016/0895-9811(96)00023-5

Bektaş, O. (1981). Kuzey Anadolu Fay Zonunun Erzincan-Tanyeri bucağı yöresindeki jeolojik özellikleri ve yerel ofiyolit sorunları (Doctoral dissertion). Karadeniz Üniversitesi Fen Bilimleri Enstitüsü, 196 pp (in Turkish with English abstract).

Bektaş, O., Şen, C., Atıcı, Y., & Köprübaşı, N. (1999). Migration of the Upper Cretaceous subduction-related volcanism toward the back-arc basin of the eastern Pontide magmatic arc (NE Turkey). *Geological Journal*, *34*(1-2), 95–106. https://doi.org/10.1002/(SICI)1099-1034(199901/06)34:1/2<95::AID-GJ816>3.0.CO;2-J

Bingöl, E., Akyürek, B., & Korkmazer, B. (1975). Biga yarımadasının jeolojisi ve Karakaya Formasyonunun bazı özellikleri. *Maden Tetkik ve Arama Enstitüsü (MTA) Publications*, 70–77. (in Turkish with English abstract)

Blumenthal, M.M. (1950). Beitraege zur geologie des landschtten am mittleren und underen Yeşilırmak (Tokat, Amasya, Havza, Erbaa, Niksar). *MTA Yayınları*, Seri D, No 4.

Boynton, W. V. (1984). Cosmochemistry of rare earth elements: Meteorite studies. In P. Henderson (Ed.), *Rare earth element geochemistry*, (pp. 63–114). Amsterdam: Elsevier. https://doi.org/10.1016/B978-0-444-42148-7.50008-3

Bustamante, C., Archanjo, C. J., Cardona, A., & Vervoort, J. D. (2016). Late Jurassic to Early Cretaceous plutonism in the Colombian Andes: A record of long-term arc maturity. *Geological Society of America Bulletin*, *11*(12), 1762–1779.

Çapan, U., & Floyd, P. (1985). Geochemical and petrographic features of metabasalts within units of the Ankara melange, Turkey. *Ofioliti*, *10*, 3–18.

Çapkınoğlu, Ş., & Bektaş, O. (1997). The Early Devonian and Permian limestone olistoliths from the Karasenir Formation, Amasya, Northern Turkey. *Geosound*, *30*, 107–115. (in Turkish with English abstract)

Catlos, E. J., Huber, K., & Shin, T. A. (2013). Geochemistry and geochronology of meta-igneous rocks from the Tokat massif, north-central Turkey: Implications for Tethyan reconstructions. *International Journal of Earth Sciences (Geologische Rundschau)*, *102*(8), 2175–2198. https://doi.org/10.1007/s00531-013-0918-0

Cherniak, D. J. (1993). Lead diffusion in titanite and preliminary results on the effects of radiation damage on Pb transport. *Chemical Geology*, *110*(1-3), 177–194. https://doi.org/10.1016/0009-2541(93)90253-F

Cox, K. G., Bell, J. D., & Pankhurst, R. J. (1979). *The interpretation of igneous rocks*. London: Allen and Unwin. https://doi.org/10.1007/978-94-017-3373-1

Dewey, J. F., Pitman, W. C., Ryan, W. B. F., & Bonin, J. (1973). Plate tectonics and the evolution of the Alpine system. *Geological Society of America Bulletin*, *84*(10), 3137–3180. https://doi.org/10.1130/0016-7606(1973)84<3137:PTATEO>2.0.CO;2

Diener, J. F. A., Powell, R., & White, R. W. (2008). Quantitative phase petrology of cordierite-orthoamphibole gneisses and related rocks. *Journal of Metamorphic Geology*, *26*(8), 795–814. https://doi.org/10.1111/j.1525-1314.2008.00791.x

Dilek, Y., Imamverdiyev, N., & Altunkaynak, Ş. (2010). Geochemistry and tectonics of Cenozoic volcanism in the Lesser Caucasus (Azerbaijan) and the peri-Arabian region: Collision-induced mantle dynamics and its magmatic fingerprint. *International Geology Review*, *52*(4–6), 536–578. https://doi.org/10.1080/00206810903360422

Dokuz, A. (2011). A slab detachment and delamination model for the generation of Carboniferous high-potassium I-type magmatism in the Eastern Pontides, NE Turkey: The Köse composite pluton. *Gondwana Research*, *19*(4), 926–944. https://doi.org/10.1016/j.gr.2010.09.006

Eyuboglu, Y. (2006). Description and geotectonic important of the Alaskan-Type mafic-ultramafic rocks in the Eastern Pontide Magmatic Arc, NE Turkey, (Doctoral dissertion). Karadeniz Teknik Üniversitesi Fen Bilimleri Enstitüsü, 205 pp (in Turkish with English abstract).

Eyuboglu, Y. (2010). Late Cretaceous high-K volcanism in the eastern Pontide Orogenic Belt, and its implications for the geodynamic evolution of NE Turkey. *International Geology Review*, *52*(2–3), 142–186. https://doi.org/10.1080/00206810902757164

Eyuboglu, Y. (2015). Petrogenesis and U-Pb zircon chronology of felsic tuffs interbedded with turbidites (Eastern Pontides Orogenic Belt, NE Turkey): Implications for Mesozoic geodynamic evolution of the Eastern Mediterranean Region and accumulation rates of turbidite sequences. *Lithos*, *212-215*, 74–92.

Eyuboglu, Y., Bektaş, O., & Pul, D. (2007). Mid-Cretaceous olistostromal ophiolitic melange developed in the back-arc basin of the Eastern Pontide magmatic arc (NE Turkey). *International Geology Review*, *49*(12), 1103–1126. https://doi.org/10.2747/0020-6814.49.12.1103

Eyuboglu, Y., Chung, S. L., Dudas, F. O., Santosh, M., & Akaryalı, E. (2011). Transition from shoshonitic to adakitic magmatism in the Eastern Pontides, NE Turkey: Implications for slab window melting. *Gondwana Research*, *19*(2), 413–429. https://doi.org/10.1016/j.gr.2010.07.006

Eyuboglu, Y., Dilek, Y., Bozkurt, E., Bektaş, O., Rojay, B., & Şen, C. (2010). Structure and geochemistry of an Alaskan-type ultramafic–mafic complex in the eastern Pontides, NE Turkey. *Gondwana Research*, *18*(1), 230–252. https://doi.org/10.1016/j.gr.2010.01.008

Eyuboglu, Y., Dudas, F. O., Santosh, M., Gümrük, T. E., Akbulut, K., Yi, K., & Chatterjee, N. (2018). The final pulse of the Early Cenozoic adakitic activity in the Eastern Pontides Orogenic Belt (NE Turkey): An integrated study on the nature of transition from adakitic to non-adakitic magmatism in a slab window setting. *Journal of Asian Earth Sciences*, *157*, 141–165. https://doi.org/10.1016/j.jseaes.2017.07.004

Eyuboglu, Y., Dudas, F. O., Santosh, M., Xiao, Y., Yi, K., Chatterjee, N., et al. (2016). Where are the remnants of a Jurassic Ocean in the Eastern Mediterranean Region? *Gondwana Research*, *33*, 63–91. https://doi.org/10.1016/j.gr.2015.08.017

Eyuboglu, Y., Dudas, F. O., Santosh, M., Yi, K., Kwon, S., & Akaryalı, E. (2013). Petrogenesis and U-Pb zircon chronology of adakitic porphyries within the Kop ultramafic massif (Eastern Pontides Orogenic Belt, NE Turkey). *Gondwana Research*, *24*(2), 742–766. https://doi.org/10.1016/j.gr.2012.11.014

Eyuboglu, Y., Dudas, F. O., Santosh, M., Zhu, D. C., Yi, K., Chatterjee, N., et al. (2016). Cenozoic forearc gabbros from the northern zone of the Eastern Pontides Orogenic Belt, NE Turkey: Implications for slab window magmatism and convergent margin tectonics. *Gondwana Research*, *33*, 160–189. https://doi.org/10.1016/j.gr.2015.07.006

Eyuboglu, Y., Dudas, F. O., Thorkelson, D., Zhu, D. C., Liu, Z., Chatterjee, N., et al. (2017). Eocene granitoids of northern Turkey: Polybaric magmatism in an evolving arc–slab window system. *Gondwana Research*, *50*, 311–345. https://doi.org/10.1016/j.gr.2017.05.008

Eyuboglu, Y., Santosh, M., Bektaş, O., & Chung, S. L. (2011). Late Triassic subduction-related ultramafic-mafic magmatism in the Amasya region (eastern Pontides, N. Turkey): Implications for the ophiolite conundrum in Eastern Mediterranean. *Journal of Asian Earth Sciences*, *42*(3), 234–257. https://doi.org/10.1016/j.jseaes.2011.01.007

Eyuboglu, Y., Santosh, M., & Chung, S. L. (2011). Petrochemistry and U-Pb ages of adakitic intrusions from the Pulur massif (Eastern Pontides, NE Turkey): Implications for slab roll-back and ridge subduction associated with Cenozoic convergent tectonics in eastern Mediterranean. *Journal of Geology*, *119*(4), 394–417. https://doi.org/10.1086/660158

Eyuboglu, Y., Santosh, M., Dudas, F. O., Akaryali, E., Chung, S. L., Akdag, K., & Bektas, O. (2013). The nature of transition from adakitic to non-adakitic magmatism in a slab-window setting: A synthesis from the eastern Pontides, NE Turkey. *Geoscience Frontiers*, *4*(4), 353–375. https://doi.org/10.1016/j.gsf.2012.10.001

Eyuboglu, Y., Santosh, M., Dudas, F. O., Chung, S. L., & Akaryalı, E. (2011). Migrating magmatism in a continental arc: Geodynamics of the Eastern Mediterranean revisited. *Journal of Geodynamics*, *52*(1), 2–15. https://doi.org/10.1016/j.jog.2010.11.006

Eyuboglu, Y., Santosh, M., Yi, K., Bektaş, O., & Kwon, S. (2012). Discovery of Miocene adakitic dacite from the Eastern Pontides Belt and revised geodynamic model for the late Cenozoic Evolution of eastern Mediterranean region. *Lithos*, *146-147*, 218–232. https://doi.org/10.1016/j.lithos.2012.04.034

Eyuboglu, Y., Santosh, M., Yi, K., Tüysüz, N., Korkmaz, S., Akaryalı, E., et al. (2014). The Eastern Black Sea-Type volcanogenic massive sulfide deposits: Geochemistry, zircon U-Pb geochronology and an overview of the geodynamics of ore genesis. *Ore Geology Reviews*, *59*, 29–54. https://doi.org/10.1016/j.oregeorev.2013.11.009

Genç, Ş. C. (2004). A Triassic large igneous province in the Pontides, northern Turkey: Geochemical data for its tectonic setting. *Journal of Asian Earth Sciences*, *22*(5), 503–516. https://doi.org/10.1016/S1367-9120(03)00090-7

Genç, Ş. C., & Yılmaz, Y. (1995). Evolution of the Triassic continental margin, Northwest Anatolia. *Tectonophysics*, *243*(1-2), 193–207. https://doi.org/10.1016/0040-1951(94)00198-I

GeoRoc (2017). georoc.mpch-mainz.gwdg.de, accessed January, 2017.

Gilbert, M. C., Helz, R. T., Popp, R. K., & Spear, F. S. (1982). Experimental studies of amphibole stability. *Reviews in Mineralogy and Geochemistry*, *9B*, 229–353.

Golonka, J., Embry, A., & Krobicki, M. (2018). Late Triassic global plate tectonics. The Late Triassic World. *Topics on Geobiology*, *46*, 27–58. https://doi.org/10.1007/978-3-319-68009-5_2

Göncüoğlu, M. C., Nurhan, T., Sentürk, K., Özcan, S., & Uysal, A. (2000). A georaverse across NW Turkey: Tectonic units of the Central Sakarya region and their tectonic evolution. *Geolological Society London, Special Publications*, *173*(1), 139–161. https://doi.org/10.1144/GSL.SP.2000.173.01.06

Gücer, M. A., Arslan, M., Sherlock, S., & Heaman, L. M. (2016). PermoCarboniferous granitoids with Jurassic high temperature metamorphism in Central Pontides, Northern Turkey. *Minerology and Petrology*, *110*(6), 943–964. https://doi.org/10.1007/s00710-016-0443-5

Hanson, G. N., & Langmuir, C. H. (1978). Modelling of major elements in mantle-melt systems using trace element approaches. *Geochimica et Cosmochima Acta*, *42*(6), 725–741. https://doi.org/10.1016/0016-7037(78)90090-X

Harley, S. L., Kelly, N. M., & Möller, A. (2007). Zircon behavior and the thermal histories of mountain chains. *Elements*, *3*(1), 25–30. https://doi.org/10.2113/gselements.3.1.25

Harrison, T. M. (1981). Diffusion of ^{40}Ar in hornblende. *Contributions to Mineralogy and Petrology*, *78*, 324–331.

Heaman, L., & Parrish, R. (1991). U-Pb geochronology of accessory minerals. *Mineralogical Association of Canada*, short course. *Notes*, *19*, 59–102.

Hervé, F., Munizaga, F., Parada, M. A., Brook, M., Pankhurst, R., Snelling, N., & Drake, R. (1988). Granitoids of the Coast Range of central Chile: Geochronology and geologic setting. *Journal of South American Earth Sciences*, *1*(2), 185–194. https://doi.org/10.1016/0895-9811(88)90036-3

Hervé, F., Pankhurst, R. J., Fanning, C. M., Calderón, M., & Yaxley, G. M. (2007). The South Patagonian batholith: 150 my of granite magmatism on a plate margin. *Lithos*, *97*(3-4), 373–394. https://doi.org/10.1016/j.lithos.2007.01.007

Karslı, O., Chen, B., Aydın, F., & Şen, C. (2007). Geochemical and Sr-Nd-Pb isotopic compositions of the Eocene Dölek and Sarıçiçek Plutons, Eastern Turkey: Implications for magma interaction in the genesis of high-K calc-alkaline granitoids in a post-collision extensional setting. *Lithos*, *98*(1-4), 67–96. https://doi.org/10.1016/j.lithos.2007.03.005

Karslı, O., Dokuz, A., Kaliwoda, M., Uysal, I., Aydin, F., Kandemir, R., & Fehr, K. T. (2014). Geochemical fingerprints of Late Triassic calc-alkaline lamprophyres from the Eastern Pontides, NE Turkey: A key to understanding lamprophyre formation in a subduction-related environment. *Lithos*, *196*, 181–197.

Kaygusuz, A., Arslan, M., Siebel, W., Sipahi, F., & Ilbeyli, N. (2012). Geochronological evidence and tectonic significance of Carboniferous magmatism in the southwest Trabzon area, eastern Pontides, Turkey. *International Geology Review*, *54*(15), 1776–1800. https://doi.org/10.1080/00206814.2012.676371

Kaygusuz, A., Arslan, M., Sipahi, F., & Temizel, İ. (2016). U–Pb zircon chronology and petrogenesis of carboniferous plutons in the northern part of the Eastern Pontides, NE Turkey: Constraints for Paleozoic magmatism and geodynamic evolution. *Gondwana Research*, *39*, 327–346. https://doi.org/10.1016/j.gr.2016.01.011

Kaygusuz, A., & Öztürk, M. (2015). Geochronology, geochemistry, and petrogenesis of the Eocene Bayburt intrusions, eastern Pontide, NE Turkey: Implications for lithospheric mantle and lower crustal sources inthe high-K calc-alkaline magmatism. *Journal of Asian Earth Sciences*, *108*, 97–116. https://doi.org/10.1016/j.jseaes.2015.04.017

Ketin, İ. (1966). Tectonic units of Anatolia. *Mineral Research and Exploration Institute of Turkey (MTA) Bulletin*, *66*, 23–34.
Koçyigit, A. (1987). Tectonostratigraphy of the Hasanoglan (Ankara) region: Evolution of the Karakaya orogenic belt. *Yerbilimleri*, *14*, 269–294. (in Turkish with English abstract)
Leake, E. B., Wooley, A. R., Arps, C. E. S., Birch, W. D., Gilbert, M. C., Grice, J. D., et al. (1997). Nomenclature of amphiboles report of the subcommittee on amphiboles of the International Mineralogical Association Commission on New Minerals and Mineral Names. *European Journal of Mineralogy*, *9*(3), 623–651. https://doi.org/10.1127/ejm/9/3/0623
Maden, N. (2013). Geothermal structure of the eastern Black Sea basin and the eastern Pontides orogenic belt: Implications for subduction polarity of Tethys oceanic lithosphere. *Geoscience Frontiers*, *4*(4), 389–398. https://doi.org/10.1016/j.gsf.2013.02.001
Maden, N., Gelişli, K., Bektaş, O., & Eyuboglu, Y. (2009). Two-and-three-dimensional crustal thickness of the Eastern Pontides (NE Turkey). *Turkish Journal of Earth Sciences*, *18*, 225–238.
McCulloch, M. T., & Black, L. P. (1984). Sm-Nd isotopic systematics of Enderby Land granulites and evidence for the redistribution of Sm and Nd during metamorphism. *Earth and Planetary Science Letters*, *71*(1), 46–58. https://doi.org/10.1016/0012-821X(84)90051-7
Morimoto, M., Fabries, J., Ferguson, A. K., Ginzburg, I. V., Ross, M., Seifert, F. A., et al. (1988). Nomenclature of pyroxenes. *Mineralogical Magazine*, *52*(367), 535–550. https://doi.org/10.1180/minmag.1988.052.367.15
Nzegge, O. M., Satır, M., Siebel, W., & Taubald, H. (2006). Geochemical and isotopic constraints on the genesis of the late Palaeozoic Delikta¸s and Sivrikaya granites from the Kastamonu granitoid belt (Central Pontides, Turkey). *Neues Jahrbuch für Mineralogie (Abhandlungen)*, *183*, 27–40.
Okay, A., & Monie, P. (1997). Early Mesozoic subduction in the eastern Mediterranean: Evidence from Triassic eclogite in northwest Turkey. *Geology*, *25*(7), 595–598. https://doi.org/10.1130/0091-7613(1997)025<0595:EMSITE>2.3.CO;2
Okay, A. I. (1984). The geology of the Ağvanis metamorphic rocks and neighbouring formations. *Bulletin. Mineral Research and Exploration Institute (Turkey)*, *99-100*, 16–36.
Okay, A. I. (1996). Granulite facies gneisses from the Pulur region, Eastern Pontides. *Turkish Journal of Earth Sciences*, *5*, 55–61.
Okay, A. I. (2000). Was the Late Triassic orogeny in Turkey caused by the collision of an oceanic plateau? *Geological Society of London, Special Publication*, *173*(1), 25–41. https://doi.org/10.1144/GSL.SP.2000.173.01.02
Okay, A. I., Altıner, D., & Kılıç, A. M. (2015). Triassic limestone, turbidites and serpentinite—The Cimmeride orogeny in the central Pontides. *Geological Magazine*, *152*(03), 460–479. https://doi.org/10.1017/S0016756814000429
Okay, A. I., & Göncüoğlu, M. C. (2004). The Karakaya complex: A review of data and concepts. *Turkish Journal of Earth Sciences*, *13*, 77–95.
Okay, A. I., Monod, O., & Monie, P. (2002). Triassic blueschists and eclogites from northwest Turkey: Vestiges of the Paleo-Tethyan subduction. *Lithos*, *64*(3-4), 155–178. https://doi.org/10.1016/S0024-4937(02)00200-1
Okay, A. I., & Nikishin, A. M. (2015). Tectonic evolution of the southern margin of Laurasia in the Black Sea region. *International Geology Review*, *57*(5-8), 1051–1076. https://doi.org/10.1080/00206814.2015.1010609
Okay, A. I., & Sahintürk, Ö. (1997). Geology of the Eastern Pontides. *American Association of Petroleum Geologists Memoirs*, *68*, 291–311.
Okay, A. I., Siyako, M., & Bürkan, K. A. (1991). Geology and tectonic evolution of the Biga Peninsula, Northwest Turkey. *Bulletin of Techical University, Istanbul*, *44*, 191–256.
Okay, A. I., & Topuz, G. (2017). Variscan orogeny in the Black Sea region. *International Journal of Earth Sciences*, *106*(2), 569–592. https://doi.org/10.1007/s00531-016-1395-z
Okay, A. I., & Tüysüz, O. (1999). Tethyan sutures of northern Turkey. *Geological Society of London, Special Publication*, *156*(1), 475–515. https://doi.org/10.1144/GSL.SP.1999.156.01.22
Özcan, A., Erkan, A., Keskin, A., Keskin, E., Oral, A., Özer, S., Sümegen, M., & Tekeli, O. (1980). Amasya-Turhal arasındaki bölgenin jeolojisi. MTA Rapor no: 6722. Ankara (in Turkish).
Özdamar, Ş. (2016). Geochemistry and geochronology of late Mesozoic volcanic rocks in the northern part of the Eastern Pontide Orogenic Belt (NE Turkey): Implications for the closure of the Neo-Tethys Ocean. *Lithos*, *248-251*, 240–256. https://doi.org/10.1016/j.lithos.2016.01.007
Parada, M. A. (1990). Granitoid plutonism in central Chile and its geodynamic implications: A review. In: Kay, S.M. and Rapela, C.W. (Eds.), Plutonism from Antarctica to Alaska. *Geological Society of America Special Papers*, *241*, 51–66. https://doi.org/10.1130/SPE241-p51
Parada, M. A., Nyström, J., & Levi, B. (1999). Multiple sources for the Coastal Batholith of central Chile (31-34°S): Geochemical and Sr-Nd isotopic evidence and tectonic implications. *Lithos*, *46*(3), 505–521. https://doi.org/10.1016/S0024-4937(98)00080-2
Pearce, J. A. (1996). A user's guide to basalt discrimination diagrams. *Geological Association of Canada, short course Notes*, *12*, 79–113.
Pickett, E. A., & Robertson, A. H. F. (1996). Formation of the Late Palaeozoic–Early Mesozoic Karakaya Complex and related ophiolites in NW Turkey by Palaeotethyan subduction- accretion. *Journal of the Geolological Society*, *153*(6), 995–1009. https://doi.org/10.1144/gsjgs.153.6.0995
Pickett, E. A., & Robertson, A. H. F. (2004). Significance of the volcanogenic Nilüfer Unit and related components of the Triassic Karakaya Complex for Tethyan subduction/accretion processes in NW Turkey. *Turkish Journal of Earth Sciences*, *12*, 97–144.
Pownall, J. M., Waters, D. J., Searle, M. P., Shail, R. K., & Robb, L. J. (2012). Shallow laccolithic emplacement of the Land's End and Tregonning granites, Cornwall, U.K.: Evidence from aureole field relations and P-T modeling of cordierite-anthophyllite hornfels. *Geosphere*, *8*(6), 1467–1504. https://doi.org/10.1130/GES00802.1
Putirka, K., Johnson, M., Kinzler, R., Longhi, J., & Walker, D. (1996). Thermobarometry of mafic igneous rocks based on clinopyroxene-liquid equilibria, 0-30 kbar. *Contributions to Mineralogy and Petrology*, *123*(1), 92–108. https://doi.org/10.1007/s004100050145
Putirka, K. D. (2008). Thermometers and barometers for volcanic systems. *Reviews in Mineralogy and Geochemistry*, *69*(1), 61–120. https://doi.org/10.2138/rmg.2008.69.3
Rice, S. P., Roberson, A. H. F., Ustaömer, T., İnan, T., & Taslı, K. (2009). Late Cretaceous-Early Eocene tectonic development of the Tethyan Suture Zone in the Erzincan area, eastern Pontides, Turkey. *Geological Magazine*, *146*(04), 567–590. https://doi.org/10.1017/S0016756809006360
Ridolfi, F., & Renzulli, A. (2012). Calcic amphiboles in calc-alkaline and alkaline magmas: Thermobarometric and chemometric empirical equations valid up to 1,130 °C and 2.2 GPa. *Contributions to Mineralogy and Petrology*, *163*(5), 877–895. https://doi.org/10.1007/s00410-011-0704-6
Robertson, A. H. F., & Ustaömer, T. (2012). Testing alternative tectono-stratigraphic interpretations of the Late Palaeozoic−Early Mesozoic Karakaya complex in NW Turkey: Support for an accretionary origin related to northward subduction of Palaeotethys. *Turkish Journal of Earth Sciences*, *21*, 961–1007.
Rojay, B., & Göncüoğlu, M. C. (1997). Tectonic setting of some pre-Liassic low grade metamorphics in Northern Anatolia. *Yerbilimleri*, *19*, 109–118. (in Turkish with English abstract)
Rojay, F. B. (1993). Tectonostratigraphy and neotectonic characteristics of the southern margin of Merzifon-Suluova basin, Central Pontides, Amasya, (Doctoral dissertion). METU, 215 pp.

Ruffet, G., Féraud, G., Ballèvre, M., & Kiénast, J. R. (1995). Plateau ages and excess argon in phengites: An 40Ar–39Ar laser probe study of Alpine micas (Sesia Zone, Western Alps, northern Italy). *Chemical Geology*, *121*(1-4), 327–343. https://doi.org/10.1016/0009-2541(94)00132-R

Şahin, S.Y., Aysal, N., & Güngör, Y. (2012). Petrology, geochemistry and geochronology of the Late Variscan granitoids (Late Permian-Early Triassic) in Western Pontides, Turkey. In: Proceedings of the 34th international Geological Congress, Abstract Book.

Sayit, K., & Göncüoğlu, M. C. (2009). Geochemistry of mafic rocks of the Karakaya Complex, Turkey: Evidence for plume-involvement in the extensional oceanic regime during Middle-Late Triassic. *International Journal of Earth Sciences*, *98*(2), 367–385. https://doi.org/10.1007/s00531-007-0251-6

Sayit, K., & Göncüoğlu, M. C. (2013). Geodynamic evolution of the Karakaya Melange complex, Turkey: A review of geological and petrological constraints. *Journal of Geodynamics*, *65*, 56–65. https://doi.org/10.1016/j.jog.2012.04.009

Sayit, K., Göncüoğlu, M. C., & Furman, T. (2010). Petrological reconstruction of Triassic seamounts/oceanic islands within the Paleotethys: Geochemical implications from the Karakaya subduction/accretion complex, Northen Turkey. *Lithos*, *119*(3-4), 501–511. https://doi.org/10.1016/j.lithos.2010.08.004

Şengör, A. M. C., & Yılmaz, Y. (1981). Tethyan evolution of Turkey: A plate tectonic approach. *Tectonophysics*, *75*(3-4), 181–241. https://doi.org/10.1016/0040-1951(81)90275-4

Smedley, P. L. (1986). The relationship between calcalkaline volcanism and within-plate continental rift volcanism: Exidence from Scottish Paleozoic lavas. *Earth and Planetary Science Letters*, *76*, 113–128.

Smith, J., & Brown, W. L. (1988). *Feldspar minerals 1. Crystal structures, physical, chemical and microtextural properties*, (2nd ed.). Berlin Heidelberg New York: Springer.

Sun, S. S., & McDonough, W. F. (1989). Chemical and isotopic systematic of ocean basalts: Implications formantle composition and process. In A. D. Saunders & M. J. Norry (Eds.), *Magmatism in the ocean basins*. *Geological Society London, Special Publications, 42*, 313–345. https://doi.org/10.1144/GSL.SP.1989.042.01.19

Sunal, G., Natal'in, B., Satır, M., & Toraman, E. (2006). Paleozoic magmatic events in the Strandja Masif, NW Turkey. *Geodinamica Acta*, *19*(5), 283–300. https://doi.org/10.3166/ga.19.283-300

Tekeli, O. (1981). Subduction complex of pre-Jurassic age, northern Anatolia. *Geology*, *9*(2), 68–72. https://doi.org/10.1130/0091-7613(1981)9<68:SCOPAN>2.0.CO;2

Topuz, G., Altherr, R., Kalt, A., Satir, M., Werner, O., & Schwarz, W. H. (2004). Aluminous granulites from the Pulur complex, NE Turkey: A case of partial melting, efficient melt extraction and crystallization. *Lithos*, *72*, 183–207.

Topuz, G., Altherr, R., Schwarz, W. H., Siebel, W., Satir, M., & Dokuz, A. (2005). Post-collisional plutonism with adakite-like signatures: The Eocene Saraycik granodiorite (Eastern Pontides, Turkey). *Contributions to Mineralogy and Petrology*, *150*(4), 441–455. https://doi.org/10.1007/s00410-005-0022-y

Topuz, G., Altherr, R., Siebel, W., Schwarz, W. H., Zack, T., Hasözbeg, A., et al. (2010). Carboniferous high-potassium I-type granitoid magmatism in the Eastern Pontides: The Gümüshane pluton (NE Turkey). *Lithos*, *116*(1-2), 92–110. https://doi.org/10.1016/j.lithos.2010.01.003

Topuz, G., Okay, A. I., Altherr, R., Schwarz, W. H., Sunal, G., & Altınkaynak, L. (2014). Triassic warm subduction in northeast Turkey: Evidence from the Ağvanis metamorphic rocks. *Island Arc*, *23*(3), 181–205. https://doi.org/10.1111/iar.12068

Tüysüz, O. (1996). Geology of Amasya and surroundings. 11th Petroleum Congress of Turkey, Proceedings, Ankara, 32–48 (in Turkish).

Uyeda, S., & Kanamori, H. (1979). Back-arc opening and the mode of subduction. *Journal of Geophysical Research*, *84*(B3), 1049–1061. https://doi.org/10.1029/JB084iB03p01049

Watson, E. B., & Harrison, T. M. (1983). Zircon saturation revisited: Temperature and composition effects in a variety of crustal magma types. *Earth and Planetary Science Letters*, *64*(2), 295–304. https://doi.org/10.1016/0012-821X(83)90211-X

Wilson, M. (1993). Magmatism and the geodynamics of basin formation. *Sedimentary Geology*, *86*(1-2), 5–29. https://doi.org/10.1016/0037-0738(93)90131-N

Yılmaz, A., & Yılmaz, H. (2004). Geology and structural evolution of the Tokat massif (eastern Pontides, Turkey). *Turkish Journal of Earth Sciences*, *13*, 231–246.

Yılmaz, Y., Tüysüz, O., Yiğitbaş, E., Genç, Ş. C., & Şengör, A. M. C. (1997). Geology and tectonic evolution of the Pontides. *American Association of Petroleum Geologists Memoir*, *68*, 183–226.

Yuva, S. (2015). Tokat Masifi içindeki metagabroyik kayaçların petrolojisi ve jeodinamik ortamı, Amasya, KD Türkiye (master's thesis). Karadeniz Teknik Üniversitesi Fen Bilimleri Enstitüsü, 53 pp (in Turkish with English abstract).